European Journal of Medicinal Chemistry 258 (2023) 115596

Contents lists available at ScienceDirect

European Journal of Medicinal Chemistry

journal homepage: www.elsevier.com/locate/ejmech

Research paper

Design, synthesis and anti-hepatic fibrosis activity of novel diphenyl vitamin D receptor agonists

Kai Xing [1], Yue Wu [1], Fei Gao, Yupeng Dai, Chun Guan, Yu Tong, Yi Gao, Cong Wang [**], Can Zhang [*]

State Key Laboratory of Natural Medicines, Jiangsu Key Laboratory of Drug Discovery for Metabolic Diseases, Center of Advanced Pharmaceuticals and Biomaterials, China Pharmaceutical University, Nanjing, 211198, PR China

ARTICLE INFO

Keywords:
Vitamin D receptor
Hepatic stellate cells
Hepatic fibrosis
Diphenyl derivatives
Agonists

ABSTRACT

Hepatic fibrosis poses a significant threat to human health due to excessive extracellular matrix (ECM) deposition leading to liver function damage. Ligand-activated vitamin D receptor (VDR) has been identified as an effective target for hepatic fibrosis, reducing ECM by inhibiting hepatic stellate cell (HSC) activation. Here, a series of novel diphenyl VDR agonists have been rationally designed and synthesized. Among these, compounds **15b**, **16i**, and **28m** showed better transcriptional activity compared to **sw-22**, which was previously reported to be a potent non-secosteroidal VDR modulator. Moreover, these compounds exhibited outstanding efficacy to inhibit collagen deposition *in vitro*. In models of CCl_4-induced and bile duct ligation-induced hepatic fibrosis, compound **16i** showed the most significant therapeutic effect by ultrasound imaging and histological examination. Moreover, **16i** was able to repair liver tissue by reducing the expression levels of fibrosis genes and serum liver function indexes without causing hypercalcemia in mice. In conclusion, compound **16i** is a potent VDR agonist with significant anti-hepatic fibrosis action both *in vitro* and *in vivo*.

1. Introduction

Hepatic fibrosis primarily results from persistent liver injury caused by various etiologies, such as viral infection, autoimmunity, drug induction, alcohol abuse, cholestasis, or metabolic diseases. It is characterized by the excessive deposition of extracellular matrix (ECM) in the liver. If left untreated, liver fibrosis can progress to cirrhosis or even liver cancer, making it one of the leading causes of death worldwide [1–3]. However, no specific and efficient drug therapy is currently available in patients [4]. There is an urgent need for novel drug interventions to address liver fibrosis.

The activation of hepatic stellate cells (HSCs) is a pivotal event in the development of hepatic fibrosis. In normal liver tissue, HSCs maintain a non-proliferative and static phenotype. In chronic liver injury, fibrotic factors like transforming growth factor-β1 (TGF-β1) activate HSCs, causing them to transform into proliferating and migrating myofibroblasts. These myofibroblasts express α-smooth muscle actin (α-SMA) and secrete ECM components, including collagen I [5–7]. The excessive deposition of ECM leads to the development of liver fibrosis, ultimately impairing normal liver function [8,9]. Therefore, inhibiting HSC activation is a promising strategy for treating liver fibrosis [10].

Recent studies have demonstrated the high expression of the vitamin D receptor (VDR), a member of the nuclear receptor superfamily, in non-parenchymal cells such as HSCs, highlighting its significance in liver fibrosis [11]. Vitamin D analogs are well-known for their ability to regulate calcium and phosphorus metabolism, promote bone development, inhibit the proliferation of various tissue cells, and modulate immune responses through their binding to VDR [12,13]. Upon binding with vitamin D analogs, the VDR competitively occupied the chromatin binding site of Smad3 in TGF-β1/Smad pathway, thus inhibiting the expression of multiple hepatic fibrosis factors [14]. Furthermore, the spontaneous development of liver fibrosis in VDR knockout mice indicates the crucial role of VDR in fibrogenesis [15]. Moreover, VDR agonists can reduce the expression levels of hydroxyproline and fibrotic factor, effectively inhibiting the accumulation of ECM [16]. These results suggest that VDR is a potential target for the treatment of hepatic

* Corresponding author.
** Corresponding author.
E-mail addresses: wangcong@cpu.edu.cn (C. Wang), zhangcan@cpu.edu.cn (C. Zhang).
[1] These authors contributed equally to this work.

https://doi.org/10.1016/j.ejmech.2023.115596
Received 16 March 2023; Received in revised form 21 June 2023; Accepted 23 June 2023
Available online 26 June 2023

fibrosis and VDR agonists hold promise as potential drugs.

VDR agonists are primarily classified into two categories: "secosteroidal" and "non-secosteroidal" [17,18]. Thousands of secosteroidal VDR ligands have been synthesized, and some of them, such as calcitriol (**1**) and calcipotriol (**2**), have been successfully marketed as drugs for osteoporosis or psoriasis [19,20]. However, they are not suitable for treating hepatic fibrosis due to their complex synthesis, unstable structure, short half-life, and potential to cause hypercalcemia [21]. To overcome these challenges, non-secosteroidal VDR agonists with high efficiency and low toxicity have been extensively investigated in recent years [22,23]. Currently, numerous non-secosteroidal VDR agonists have been reported, such as derivatives of bisphenol cyclo methanes (**3**) [24], phenylpyrrorole pentanes (**4**) [25], trichromatic cycloalcohols (**5**) [26] and carborane (**6**) [27] (Fig. 1). Previously, our group conducted a series of studies on phenylpyrrole pentane derivatives, which exhibited strong VDR affinity and the ability to inhibit multicellular proliferation without affecting serum calcium levels [28,29]. However, there is a need to enhance the ability to inhibit the activation of HSCs [30].

In this study, to further enhance the anti-fibrotic activity of non-secosteroidal VDR agonists, we conducted a preliminary analysis of the structural characteristics of secosteroidal and non-secosteroidal compounds. Based on previous descriptions [31], we proposed that the conjugated triene system in secosteroidal compounds might be responsible for the hypercalcemia effect, which was avoided in our subsequent design. Additionally, we observed that although the non-secosteroidal compounds mimicked the hydroxyl activity at the C1 and C25 positions of calcitriol, they lacked sufficient interaction force at the C3 hydroxyl group, which could explain their reduced potency. To address this, we sought to strengthen the bonding force by increasing the hydrogen bonding sites by simulating the affinity at the C3 site. Considering these factors, we synthesized a total of 54 compounds and conducted various biological experiments through three rounds of modification. Among these compounds, **15b**, **16i**, and **28m** demonstrated superior performance in terms of transcriptional activity compared to the positive control **sw-22** and were comparable to calcipotriol. Notably, compound **16i** exhibited the optimal inhibitory activity on fibrosis gene expression and collagen deposition. Histological analysis further demonstrated the effectively of compound **16i** in preventing liver fibrosis induced by both carbon tetrachloride (CCl_4) and bile duct ligation (BDL) in mice. Importantly, compound **16i** had no significant effect on serum calcium levels.

2. Results and discussion

2.1. Structural design of the compounds

Remarkably, a study demonstrated that compounds derived from preserving the A ring of calcitriol, arylation of CD ring, and incorporation of distinct lengths of alkyl substituents into the triene system exhibited excellent transcriptional activity [32]. Additionally, it was observed that the dihydroxymethyl phenyl structure showed superior binding affinity (74% VDR affinity compared to calcitriol) when simulating the A ring with an aromatic ring with polyhydroxyl substitution while retaining the CD ring [33]. Building upon these findings, we employed the design strategy of pharmacophore fusion and scaffold hopping to create a novel class of compounds (Fig. 2). These proposed compounds fractured three hydroxyl groups capable of establishing crucial hydrogen bond forces, and the central double bond in the structure facilitated the maintenance of the trans conformation, mimicking the spatial orientation of calcitriol. The side chains were connected by flexible ether bonds as linkers, and a comprehensive Structure-Activity Relationship (SAR) evaluation was conducted.

2.2. Chemistry

The synthetic pathway of the target compounds **15a-l** and **16a-i** is outlined in Scheme 1. Intermediate **2** was synthesized by reacting compound **1**, which possessed either a meta-hydroxyl or para-hydroxyl group, with tert-butyldimethylchlorosilane. Meanwhile, commercially available compound **3** was hydrolyzed with NaOH to obtain compound **4**, which was then esterified with ethanol to yield intermediate **5**. Compound **6** was obtained through the reflux reaction of intermediate **5** with NBS in a CCl_4 solution at 90 °C catalyzed by AIBN. Subsequently, compound **6** was coupled with compound **2** through Wittig-Horner reaction form intermediate **8**. The deprotection reaction of intermediate **8** yielded compound **9**, which was reduced using $LiAlH_4$ to obtain compound **10**. The two benzyl hydroxyl groups of compound **10** were protected to form acetal compound **11**. On one hand, under the condition of

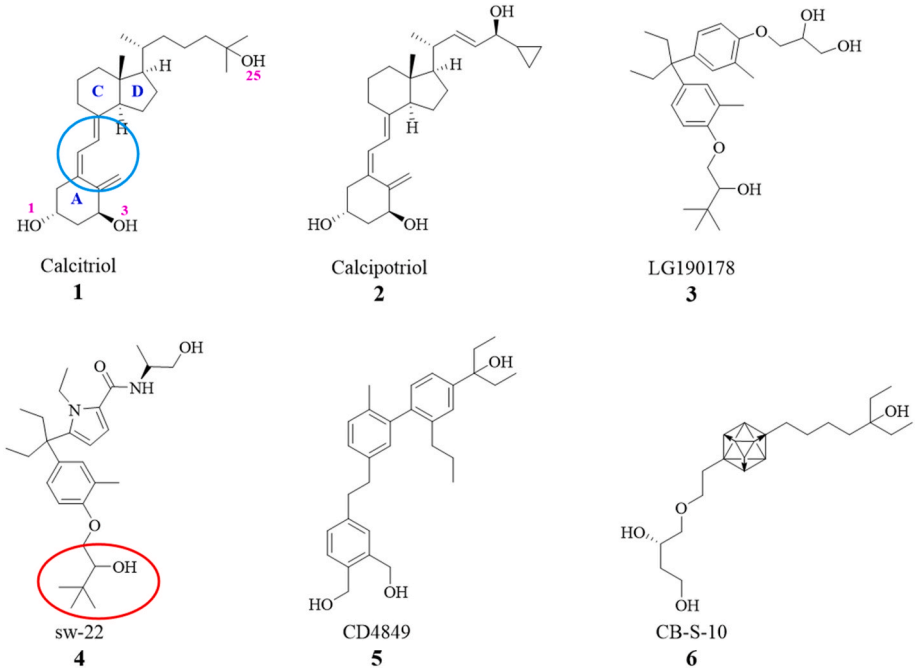

Fig. 1. Chemical structures of representative VDR agonists.

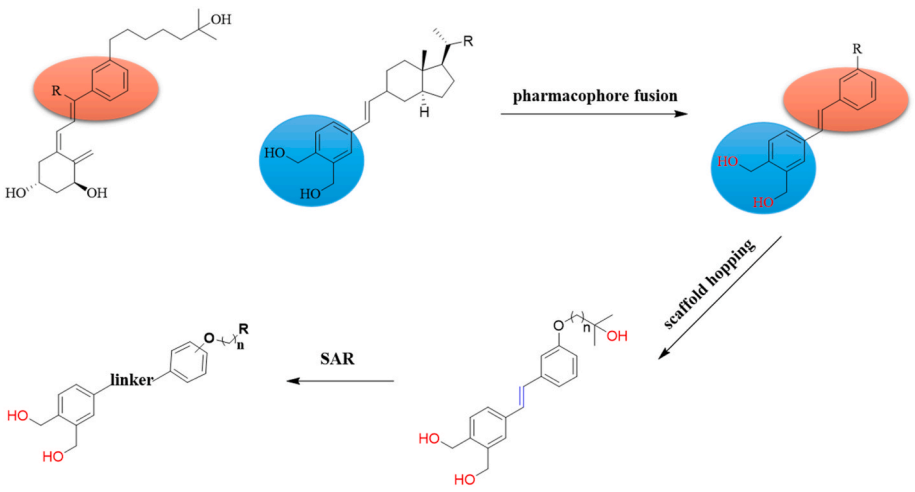

Fig. 2. Rational drug design of VDR agonists.

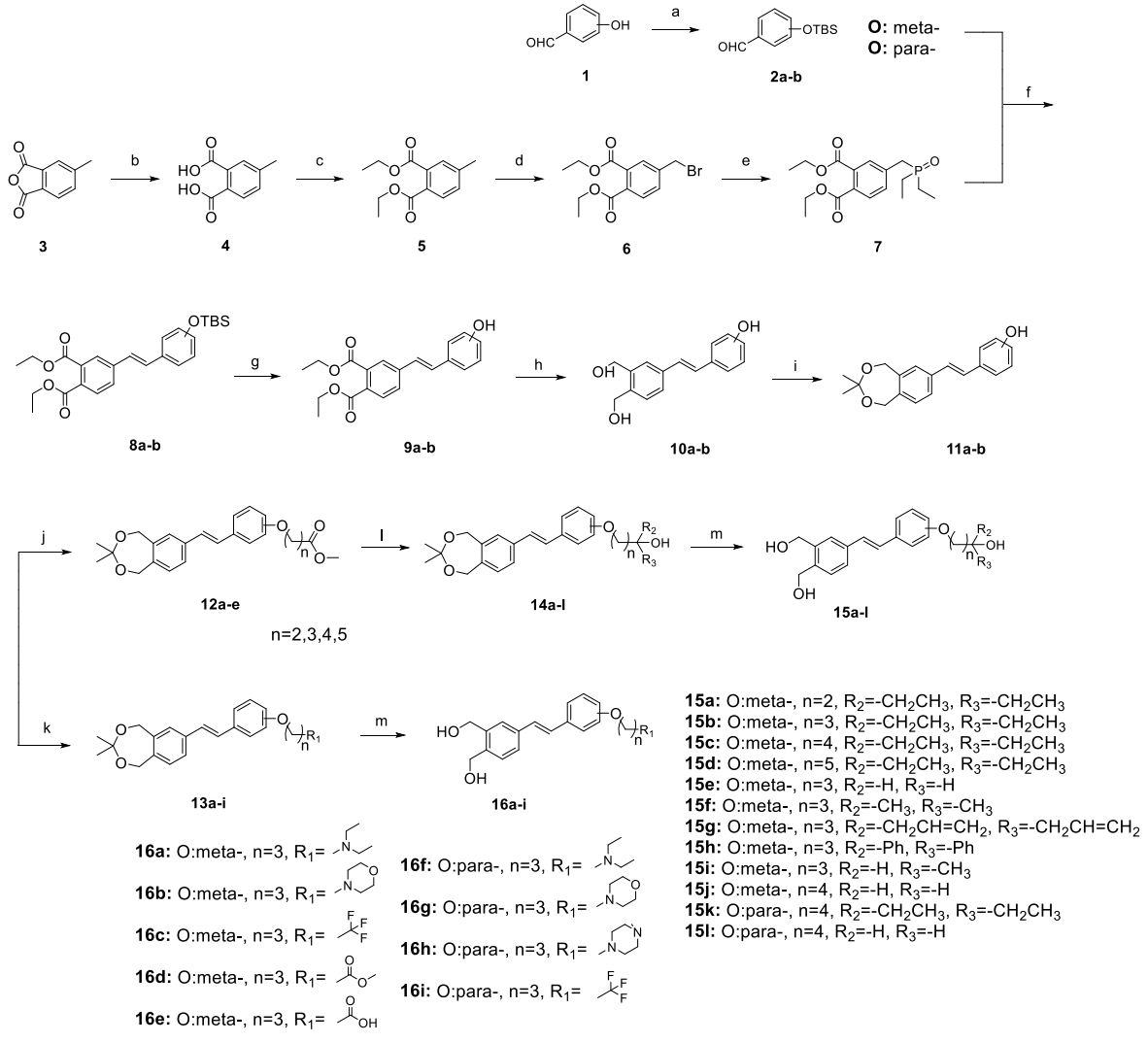

Scheme 1. Synthesis of target compounds **15a-l** and **16a-i**.
[a]Reagents and conditions: (a) TBSCl, CH_2Cl_2, rt, 30 min; (b) NaOH, H_2O–CH_3OH (1:5), rt, 30 min; (c) C_2H_5OH, conc. H_2SO_4, reflux, 8 h; (d) NBS, AIBN, CCl_4, reflux, 6 h; (e) Triethyl phosphite, 120 °C, 5 h; (f) NaH, THF, rt, overnight; (g) TBAF, THF, rt, 30 min; (h) $LiAlH_4$, THF, 0 °C, 3 h; (i) *p*-TOS, 2,2-Dimethoxypropane, Acetone, rt, 45 min; (j) NaH, DMF, rt, 3 h; (k) PPh_3, DEAD, THF, 0 °C - rt, overnight, N_2 atmosphere; (l) RMgBr, THF, 0 °C, overnight, N_2 atmosphere; (m) *p*-TOS, THF, rt, 1 h.

NaH, the phenolic hydroxyl group of **11** was substituted with various halogenated esters in DMF, leading to the synthesis of compound **12**, which was then converted to tertiary alcohol compound **14** via a Grignard reaction. On the other hand, intermediate **11** was coupled with different amines, esters, and acids in a single step to produce compound **13**. The target compounds **15a-l** and **16a-i** were obtained by deprotecting compounds **13** and **14** under acidic conditions.

The synthetic route for the target compounds **17a-h** is outlined in Scheme 2. The target compounds **17a-h** were synthesized from compound **15** by a diimide reduction reaction.

The synthetic route for the target compounds **28a-p** and **29a-i** are outlined in Scheme 3. The aldehyde group of the starting material **2** was reacted with different alkyl-Grignard reagents to produce compound **18**. Meanwhile, compound **19** was esterified with ethanol to give compound **20**. Compound **20** and compound **18** were coupled through the Mitsunobu reaction to afford intermediate **21**, which was deprotected with tetrabutylammonium fluoride to obtain compound **22**. The subsequent steps were then performed as described in Scheme 1, and the target compounds **28a-p** and **29a-i** were finally obtained.

2.3. VDR binding affinity

The structures of synthesized compounds are presented in Table 1. To determine the VDR binding ability of the synthesized compounds, ligand competitive binding tests were conducted. Calcipotriol as a positive control and the binding force was defined as 100%. The relative affinity of the target compounds at the concentration of 1 μM was calculated using the following formula: Relative affinity (%) = (mP_{DMSO} - $mP_{Compound}$)/(mP_{DMSO} - $mP_{Calcipotriol}$) × 100%. As shown in Table 2, several compounds exhibited outstanding VDR affinity. Among them, compounds **16i** and **28m** showed an inhibition rate of more than 50% on the fluorescent VDR ligand. Based on these results, it can be concluded that the VDR affinity of the compounds was greatly influenced by the terminal group type, substitution position, linker, and introduction of intermediate hydrophobic fragments.

2.4. CYP24A1 transcriptional ability

To further assess the VDR activation ability and anti-fibrotic effect of compounds *in vitro*, human LX-2 cells were utilized for subsequent experiments [34]. Considering the potential cytotoxicity effect on HSC activation, the toxicity of all compounds on LX-2 cells was detected by CCK-8 assay. As shown in Table S1, the IC_{50} values of compounds were greater than 30 μM, which means the compounds had few obvious toxic effects on LX-2 cells.

The VDR-down-stream-target gene *CYP24A1*, severing as the marker of transcriptional activity, is highly expressed after activation of VDR [35]. In previous studies, non-secosteroidal VDR agonists achieved a good VDR activation effect at the concentration of around 0.5 μM [36]. Considering both safety and effectiveness, we ultimately chose 0.5 μM as the administration concentration for *in vitro* experiments.

The expression of *CYP24A1* in human HSCs LX-2 was detected by qPCR and the results are shown in Fig. 3 and Fig. S1. The modification of compounds began with the length of the side chain, and the widely reported ethyl tertiary alcohol was used as the terminal group to investigate the interaction of different chain lengths at the meta-position of the benzene ring with the protein residues [26,27]. *In vitro,* VDR affinity (Table 2) and *CYP24A1* mRNA expression showed that the chain length activity sequence was observed as 3 > 5>2 > 4. Additionally, compound **15b** exhibited the same binding affinity and activation activity as **sw-22**.

Due to the dominance of **15b** in transcriptional activity, we retained the side chain length with three carbons and screened for different types of terminal groups. In terms of optimizing hydrophobic action, when the terminal substituent retained the tertiary alcohol form, phenyl, allyl, and methyl were introduced respectively to increase or decrease steric hindrance. The binding force and activation ability of compounds **15f**-**15h** were weaker than those of **15b**. Furthermore, the activity decreased when primary and secondary alcohols (**15e**, **15i**) were substituted for tertiary alcohols to reduce the hydrophobic force around the end group. However, the transcriptional efficiency was equivalent to that of **15b** when the trifluoromethyl group was applied as a bio isosteric replacement (**16c**). Regarding the optimization of esterophilic and hydrophilic properties, esters and acids were selected for further research. The acids showed outstanding activation effects, which might be related to the interaction between water molecules and hydrogen bond donors. Although a series of studies on the end groups had been conducted, their activity still needed improvement. Considering the reduced activity caused by the compound properties of the compound, such as water solubility and molecular polarity, we modified the end group with a nitrogen heterocycle [37]. The open diethylamine group was found to be superior to the closed morpholine group (**16a**, **16b**). However, the transcriptional activity was still unsatisfactory, probably due to their unfavorable interaction with the hydrophobic capsule in the protein-binding site. Hence, we focused on the substituent potency of the side chain at the para-position of the benzene ring. Based on molecular docking simulations, structural optimizations were performed according to the aforementioned three aspects, among which **16i** exhibited better binding and activation ability. In summary, in the first round of modification, we found that changes in end-group and side-chain positions had a limited impact on improving activity.

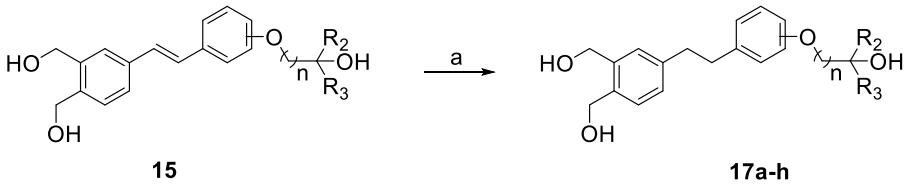

17a: O: meta-, n=3, R_2=-H, R_3=-H
17b: O: meta-, n=3, R_2=-CH_3, R_3=-CH_3
17C: O: meta-, n=3, R_2=-CH_2CH_3, R_3=-CH_2CH_3
17d: O: meta-, n=3, R_2=-$CH_2CH{=}CH_2$, R_3=-$CH_2CH{=}CH_2$
17e: O: meta-, n=3, R=-$COOCH_3$
17f: O: para-, n=4, R_2=-CH_3, R_3=-CH_3
17g: O: para-, n=4, R_2=-CH_2CH_3, R_3=-CH_2CH_3
17h: O: para-, n=4, R_2=-$CH_2CH{=}CH_2$, R_3=-$CH_2CH{=}CH_2$

Scheme 2. Synthesis of target compounds **17a-h**.
[a]Reagents and conditions: (a) 4-Methylbenzenesulfonhydrazide, CH_3COONa, EtOH, reflux, 8 h.

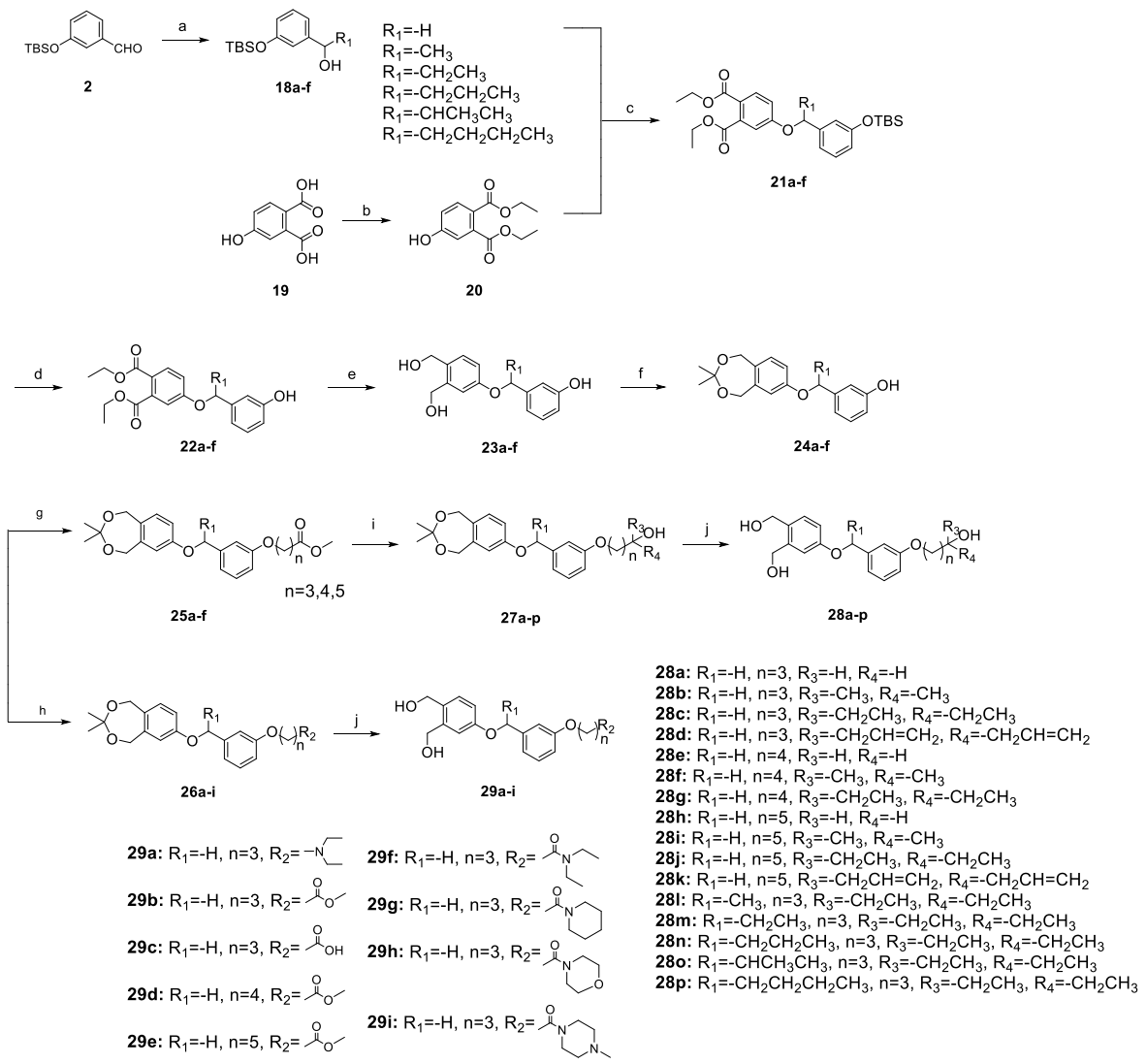

Scheme 3. Synthesis of target compounds **28a-p** and **29a-i**.
[a]Reagents and conditions: (a) RMgBr, THF, rt, overnight; (b) C_2H_5OH, conc. H_2SO_4, reflux, 8 h; (c) PPh_3, DEAD, THF, 0 °C - rt, overnight, N_2 atmosphere; (d) TBAF, THF, rt, 30 min; (e) $LiAlH_4$, THF, 0 °C, 3 h; (f) *p*-TOS, 2,2-Dimethoxypropane, Acetone, rt, 45 min; (g) NaH, DMF, rt, 3 h; (h) PPh_3, DEAD, THF, 0 °C - rt, overnight, N_2 atmosphere; (i) RMgBr, THF, 0 °C, overnight, N_2 atmosphere; (j) *p*-TOS, THF, rt, 1 h.

Considering that the selection of *trans*-ene as the linker allowed the molecular structure to be in a π-π fully conjugated rigid configuration, which limited the formation of the dominant conformation, we performed a flexible modification to generate C–C bonds (**17a-17h**). No significant difference was found between the experimental group and the negative control (Fig. 3). We believe that an increase in rotatable bonds is beneficial for achieving low-energy conformations, but an excessive number of them does not provide a definite energy advantage, and may alter the binding mode. Collectively, it is necessary to design compounds with a slightly flexible linker [38].

In the second round of optimization, we proceeded with semi-flexible modification by introducing oxygen-containing heteroatoms and synthesized compounds **28a-p** and **29a-i**. The results revealed that the impact of side chain length on transcriptional activity was essentially similar to that of **15a-15d**, following the sequence of 3 > 5>4. Meanwhile, it was noted that although the overall activity of the compounds with four-carbon length was generally low, they showed excellent activation ability after ester modification with prodrug at **29d**. Moreover, the effects of the terminal group hydrophobicity on the activity showed slight variability. For the compounds with n = 3, ethyl was preferred as R_2, followed by methyl, and then allyl and H. For n = 4 or 5, allyl was optimal, followed by H, ethyl, and methyl. Among them, compounds **28c** and **28k** exhibited the highest activity. Additionally, in accordance with the optimization of nitrogen-containing heterocyclic rings in the first round, compound **29a** with a diethylamine group as the end group was synthesized, but its transcriptional activity didn't improve. Therefore, amides with better stability and selectivity *in vivo* were applied (**29f-29i**) [39], and their activity remained unchanged. Finally, molecules **15b** and **28c** optimized in the first and second rounds served as the starting point for the third round of structural transformation. Numerous investigations have demonstrated that the C ring of calcipotriol and the diethyl part of **sw-22** can form hydrophobic interactions with tryptophan 282 in the protein cavity and contribute to their activity [40,41]. Consequently, we designed and synthesized the compound **28l-28p** by adding hydrophobic alkyl to displace water molecules. Compound **28m** showed superior activation ability.

After comprehensive consideration of VDR relative affinity and transcriptional activity, 20 representative compounds with excellent terminal groups, suitable chain length, and a semi-flexible linker were selected for conducting subsequent activity evaluation.

Table 1
Chemical Structures of Synthetized compounds.

Table 1.1. The structures of 15a-l, 16a-i, and 17a-h.

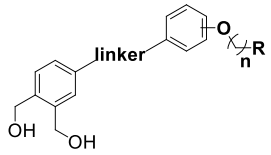

Compd.	O	n	R	linker	Compd.	O	n	R	linker
15a	meta-	2			**16d**	meta-	3		
15b	meta-	3			**16e**	meta-	3		
15c	meta-	4			**16f**	para-	3		
15d	meta-	5			**16g**	para-	3		
15e	meta-	3			**16h**	para-	3		
15f	meta-	3			**16i**	para-	3		
15g	meta-	3			**17a**	meta-	3		
15h	meta-	3			**17b**	meta-	3		
15i	meta-	3			**17c**	meta-	3		
15j	meta-	4			**17d**	meta-	3		
15k	para-	4			**17e**	meta-	3		
15l	para-	4			**17f**	para-	4		
16a	meta-	3			**17g**	para-	4		
16b	meta-	3			**17h**	para-	4		
16c	meta-	3							

Table 1.2. The structures of 28a-p and 29a-i.

Compd.	n	R_1	R_2	Compd.	n	R_1	R_2
28a	3	-H		**28n**	3	$-CH_2CH_2CH_3$	
28b	3	-H		**28o**	3	$-CHCH_3CH_3$	
28c	3	-H		**28p**	3	$-CH_2CH_2CH_2CH_3$	
28d	3	-H		**29a**	3	-H	
28e	4	-H		**29b**	3	-H	
28f	4	-H		**29c**	3	-H	
28g	4	-H		**29d**	4	-H	
28h	5	-H		**29e**	5	-H	
28i	5	-H		**29f**	3	-H	
28j	5	-H		**29g**	3	-H	
28k	5	-H		**29h**	3	-H	
28l	3	$-CH_3$		**29i**	3	-H	
28m	3	$-CH_2CH_3$					

Table 2
Relative VDR binding ability of Synthetized compounds at 1 μM.

Compd.	[a]Relative VDR binding ability (%)	Compd.	Relative VDR binding ability (%)	Compd.	Relative VDR binding ability (%)
15a	38.15029122	**16h**	21.38728447	**28j**	3.468208293
15b	47.97110104	**16i**	51.43930933	**28k**	46.24277724
15c	23.12138862	**17a**	32.36994407	**28l**	45.08670781
15d	33.5260135	**17b**	14.45086789	**28m**	54.33526326
15e	11.56069431	**17c**	28.32370106	**28n**	46.24277724
15f	44.50867309	**17d**	35.26011765	**28o**	36.41618708
15g	40.46243008	**17e**	46.24277724	**28p**	42.19653423
15h	23.69942334	**17f**	11.56069431	**29a**	49.71098553
15i	8.670520732	**17g**	44.50867309	**29b**	19.65318033
15j	5.780347155	**17h**	16.18497203	**29c**	9.248555448
15k	31.21387464	**28a**	41.61849952	**29d**	45.66474252
15l	36.41618708	**28b**	27.16763163	**29e**	29.47977049
16a	42.19653423	**28c**	43.35260366	**29f**	8.670520732
16b	34.10404821	**28d**	20.23121504	**29g**	24.85549277
16c	30.05780521	**28e**	9.826590163	**29h**	17.91907618
16d	34.10404821	**28f**	9.248555448	**29i**	30.05780521
16e	36.99422179	**28g**	35.83815236	[b]**DMSO**	0
16f	49.71098553	**28h**	9.248555448	**sw-22**	55.49133269
16g	32.36994407	**28i**	27.16763163	[c]Calcipotriol	100

[a] Results were expressed as the mean relative VDR binding ability of three experiments.
[b] DMSO was used as the negative control.
[c] Calcipotriol was used as the positive control.

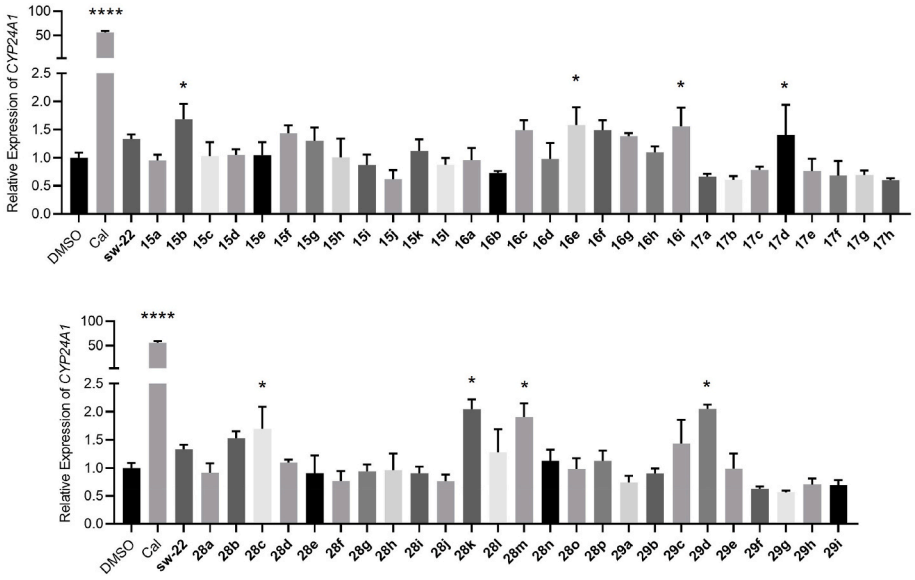

Fig. 3. The relative expression of *CYP24A1* in LX-2 cells was detected by qPCR after treatment with different compounds at a final concentration of 0.5 μM, with calcipotriol and **sw-22** as positive controls and DMSO as negative control (mean ± SD; *$P < 0.05$ vs DMSO, ****$P < 0.0001$ vs DMSO).

2.5. Transactivation

To further access the activity of the screened compounds, the VDR transactivation activity of the preferred compounds was determined in HEK293 cells using a dual-luciferase reporter assay (Fig. 4A). Calcipotriol and **sw-22** served as positive controls, while DMSO served as a negative control. Compounds **15b**, **16i,** and **28m** exhibited exceptional transcriptional activity. Subsequently, as shown in Fig. 4B, all three compounds exhibited concentration-dependent transcriptional activity and acted as effective VDR agonists. In comparison to calcipotriol, they maintained large activity even at lower concentrations, with all three compounds having significantly higher transactivation activity than **sw-22**.

2.6. Compounds inhibiting the activation of human LX-2 cells

The overexpression of collagen I and α-SMA, which are markers of hepatic fibrosis, is regarded as the primary characteristic of HSC activation. LX-2 cells were treated with different compounds at a concentration of 0.5 μM in the presence of 5 ng/mL TGF-β1 for 24 h [42]. The expression levels of collagen I and α-SMA were analyzed by western blotting. As shown in Fig. 5, TGF-β1 treatment increased the protein expression of hepatic fibrosis markers, while the expression of related proteins was effectively inhibited after the administration of some compounds. Based on the results the of anti-fibrotic activity, when the tertiary alcohol form was preserved as the terminal group, the substituent activity order was Ethyl > Methyl > H. In terms of the overall activity, the meta-position of the benzene ring was superior to the para-position, and the semi-flexible C–O bond modification was better than the rigid C═C bond. And among the other end-substituted groups,

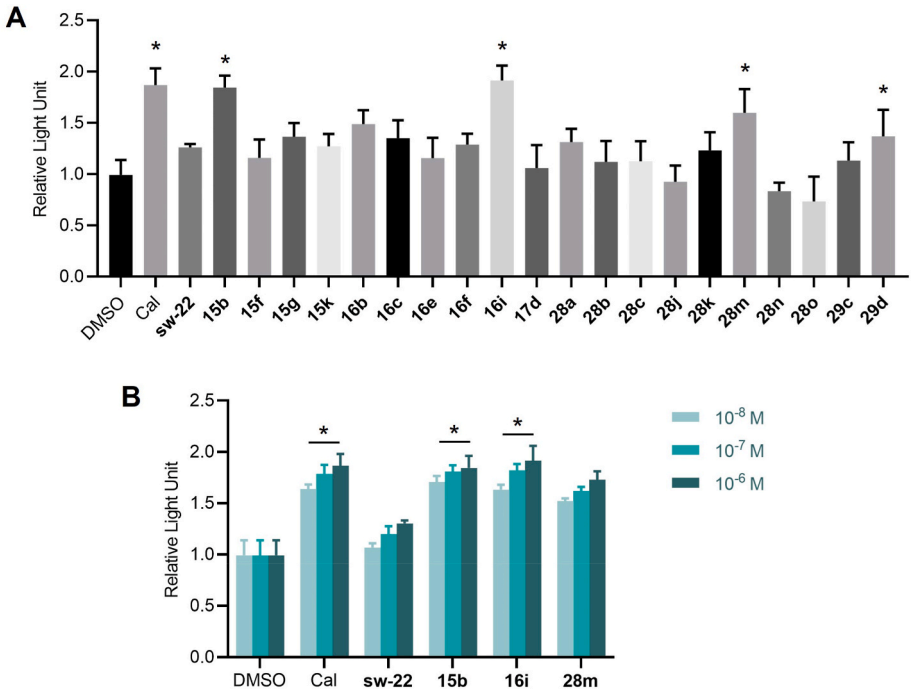

Fig. 4. The VDR transactivation activities of 20 preferred compounds were detected in HEK293 cells using dual luciferase reporter genes, with calcipotriol and **sw-22** as positive controls and DMSO as a negative control. (A) Transcriptional activities of the 20 preferred compounds at 0.5 μM (mean ± SD; $^*P < 0.05$ vs DMSO). (B) Transcriptional activities of the 3 preferred compounds at 0.01 μM, 0.1 μM and 1 μM (mean ± SD; $^*P < 0.05$ vs DMSO).

trifluoromethyl showed more efficiency than acid, ester, and nitrogen heterocyclic rings under a rigid configuration. During the screening of intermediate hydrophobic fragments, ethyl was found to be the most effective, followed by isopropyl, with propyl being the least efficient.

After multiple rounds of modification, compounds **15b**, **16i**, and **28m** exhibited better inhibition of HSC activation, which was consistent with their previous *in vitro* transcriptional activity and relative affinity for VDR. Among them, compound **28m** demonstrated similar inhibition of collagen I and α-SMA compared to the positive controls calcipotriol and **sw-22**.

2.7. Molecular docking

To gain further insight into the interaction mode between the compounds and VDR, molecular docking was performed with compounds **15b**, **16i**, and **28m** docked into the ligand-binding pocket of VDR (PDB code: 2ZFX). The docking results revealed that the **15b** could form hydrogen bonding forces with Ser233, and the tertiary alcohol hydroxyl group in the side chain made hydrogen bond interactions with His393 and His301, respectively. Interestingly, the phenyl parent nucleus of **15b** could engage in π–π stacking interactions with the indole ring of Trp282, despite its benzyl hydroxyl only forming one interaction. For compound **16i**, one benzyl hydroxyl group formed a hydrogen bonding interaction with Tyr143 and Ser274, while the other could additionally bond with Ser233 and Arg270. Meanwhile, the terminal trifluoromethyl group occupied the hydrophobic cavity effectively and formed a halogen bonding force with the amino group of His301. After multiple rounds of optimization, compound **28m** retained all the hydrogen bonding forces of **15b** and **16i**, and the ethyl fragment in the middle of the structure also formed a strong hydrophobic interaction with Trp282, whereas substituting it with other chain lengths did not receive better results. The molecular superposition of **28m** with calcipotriol and **sw-22** exhibited that spatial structure simulated the position of the 1-OH and 25-OH groups of calcipotriol, which are crucial for to binding with VDR. In addition, in line with the previous design concept, **28m** also formed a weak hydrogen bonding force similar to calcipotriol at the position of 3-OH, and the middle hydrophobic fragments occupied the binding cavity effectively (Fig. 6).

2.8. Compounds *15b*, *16i*, and *28m* improving CCl_4-induced hepatic fibrosis mice

Based on the aforementioned results *in vitro*, compounds **15b**, **16i**, and **28m** were selected for further study *in vivo*. To preliminarily evaluate the anti-fibrotic effect of these representative compounds, we established a hepatic fibrosis model in C57BL/6 mice by intraperitoneal injection of CCl_4 [43,44]. Compounds **15b**, **16i,** and **28m** were orally administered at a dosage of 500 μg/kg, five times a week for two weeks (Fig. 7A). Qualitative ultrasound imaging was performed at specified time points [45,46]. As shown in Fig. 7B and Fig. S2, CCl_4-induced mouse liver echograms showed uneven parenchymal echo, irregular liver surface, and increased brightness, indicating the development of liver of mice has developed fibrosis. However, after treatment with calcipotriol or the screened compounds, the liver parenchyma of mice became more uniform, and the brightness ratio of the liver and kidney decreased. Among them, compound **16i** exhibited the equivalent restorative effect to calcipotriol.

Previous studies have shown that the activation and *trans*-differentiation of HSCs into myofibroblasts are the main drivers of hepatic fibrosis formation. Continuous activation responses lead to excessive deposition of ECMs, further exacerbating the development of fibrosis [5–7]. To corroborate the results of ultrasound imaging, the expression levels of the myofibroblast marker fibronectin (*Fn*), as well as connective tissue growth factor (*Ctgf*) and tissue inhibitor of metalloproteinase −1 (*Timp-1*), which are associated with ECM synthesis and degradation, were further examined by qPCR [47,48]. As depicted in Fig. 7C, compared to the up-regulation observed in the CCl_4 group, the expression of *Fn*, *Ctgf*, and *Timp-1* in the livers of mice treated with compound **16i** was effectively inhibited.

Liver histopathology was examined by Hematoxylin-Eosin (H&E) staining and collagen deposition in each group was examined by Masson's Trichrome staining (Fig. 7D) [49]. The results showed that the

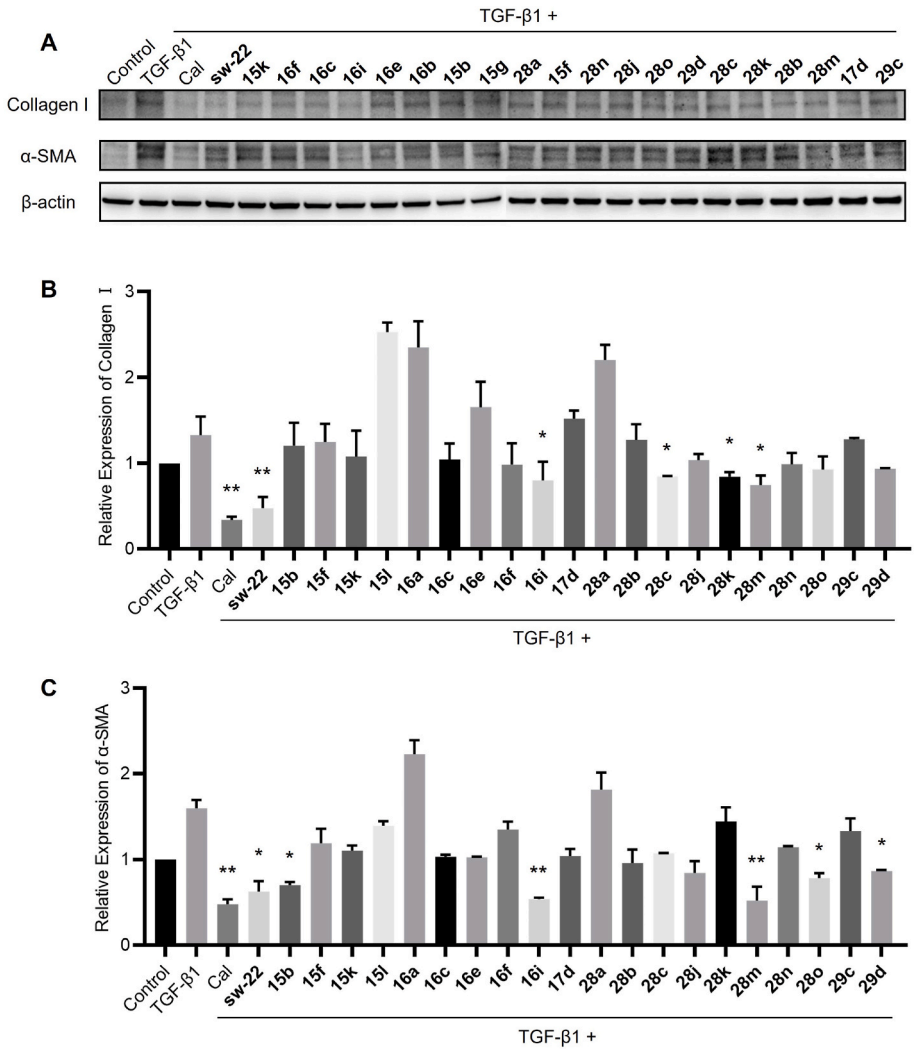

Fig. 5. Relative expression of collagen I and α-SMA in LX-2 cells was determined by Western blot, after treatment with different compounds at a final concentration of 0.5 μM, with calcipotriol and **sw-22** as positive controls and DMSO as negative control. (A) The representative gel electrophoresis bands. (B–C) Relative expression of collagen I and α-SMA proteins, normalized to the expression of β-actin protein (mean ± SD; $^{*}P < 0.05$ vs TGF-β1, $^{**}P < 0.01$ vs TGF-β1).

three representative compounds could reduce the lesions, decrease inflammatory cell infiltration, and inhibit the proliferation of fibrous tissue and collagen deposition to varying degrees (Fig. 7E). In addition, serum levels of alanine aminotransferase (ALT), aspartate aminotransferase (AST), and total bile acid (TBA) levels are commonly used clinically to assess liver health status [50]. An abnormal elevation of these indexes suggests the existence of varying degrees of liver tissue injury. As shown in Fig. 7F, CCl_4-induced mice exhibited significantly increased expression of these indicators compared to the control group. Compounds **15b**, **16i**, and **28m** were able to reduce AST, ALT, and TBA levels in mice, with compound **16i** showing a more significant effect than **sw-22**. Considering the dose-dependent hypercalcemia side effect of steroid compounds, the serum calcium concentration was measured by calcium activity assay to determine the dosage that achieved a therapeutic effect without inducing hypercalcemia with non-steroid compounds. Calcipotriol at a dose of 100 μg/kg had a significant side effect of increasing calcium levels, while compound **16i** showed minimal effect even at a dose of 500 μg/kg, as shown in Fig. 7G.

Overall, while maintaining an excellent anti-fibrosis effect, compound **16i** did not have the side effect of hypercalcemia, which differed from **28m**, which demonstrated optimal inhibition of collagen I *in vitro*. We hypothesized that compound **16i** might have a better duration and metabolic stability *in vivo*, which could be attributed to the trifluoromethyl group in the side chain, which blocks the metabolic sites of the benzene ring and tertiary alcohol respectively.

2.9. Compounds **15b**, **16i**, and **28m** improving BDL-induced hepatic fibrosis mice

Hepatic fibrosis is the consequence of sustained liver damage caused by different etiologies. Impaired bile secretion leads to cholestatic liver disease. Cholestasis is characterized by increased hepatocyte death due to elevated biliary pressure, triggering inflammation, recruitment of immune cells, HSC activation, and significant periportal fibrosis within 2–3 weeks after BDL [42]. Therefore, we further investigated the effect of the compound on a mouse model of acute liver injury induced by BDL.

BDL surgery was performed on C57BL/6 mice, followed by compound administration one week after ligation for 10 days (Fig. 8A). Ultrasonic imaging of mouse livers was observed at specified time points, and compound **16i** had a significant therapeutic effect compared to the vehicle group (Fig. 8B and Fig. S3). Similar to the CCl_4-induced liver fibrosis model, compound **16i** treatment decreased the expression of *Fn*, *Ctgf*, and *Timp-1*, as well as collagen content in the liver, and gradually alleviated the serum ALT, AST, and TBA levels (Fig. 8C–E). H&E staining of mice livers treated with compound **16i** also showed fewer lesions and less inflammatory cell infiltration as well (Fig. 8D).

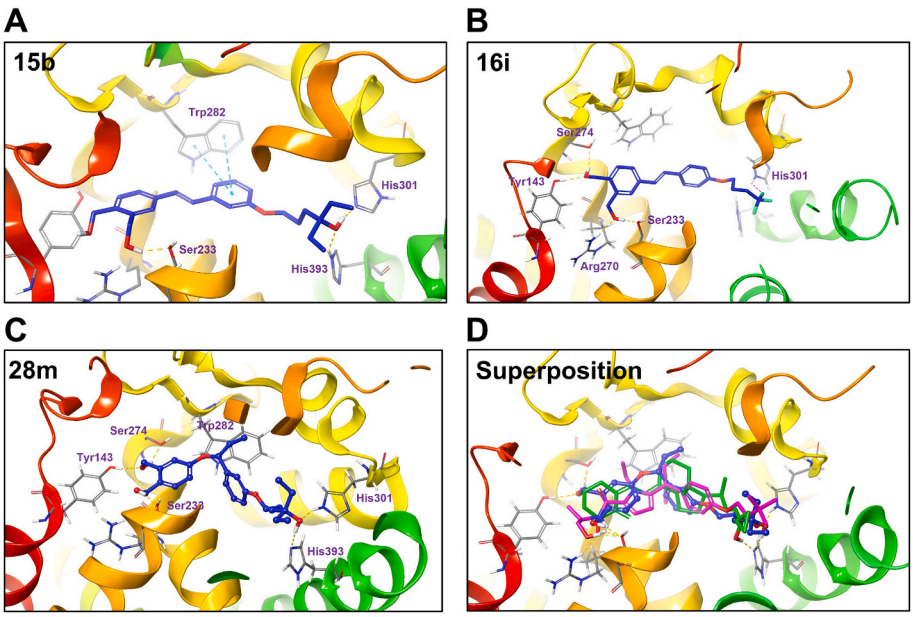

Fig. 6. Predicted binding model of **15b** (A), **16i** (B), and **28m** (C). The VDR-LBD of PDB reference 2ZFX was used in the molecular-docking analysis performed with Glide 5.5 in Schrödinger 2009. (D) Superposition of compounds **28m**, **sw-22,** and calcipotriol. Compound **28m** is depicted in blue, **sw-22** is in pink and calcipotriol is in green.

These results indicated that compound **16i** treatment could prevent BDL-induced liver injury. Moreover, it demonstrated a high degree of separation between its anti-fibrotic and calcific effects (Fig. 8F–G).

3. Conclusion

In conclusion, we synthesized 54 diphenyl derivatives based on the design concepts of pharmacophore fusion and scaffold hopping and discussed the structure-activity relationship (SAR) of these compounds. Through multiple rounds of optimization, compounds **15b**, **16i**, and **28m** optimization demonstrated excellent binding affinity to the vitamin D receptor (VDR) and transcriptional activity. *In vitro,* experiments further confirmed their ability to inhibit the activation of hepatic stellate cells (HSCs) induced by TGF-β1. Particularly, compound **16i** exhibited the most significant anti-fibrotic effect in both CCl_4-induced and BDL-induced mouse models of hepatic fibrosis. It showed superior efficacy compared to calcipotriol reducing the levels of hepatic fibrosis markers and serum liver function indexes, while effectively inhibiting extracellular matrix (ECM) deposition and liver tissue damage. The metabolic stability of compound **16i** *in vivo* contributed to this effect. Furthermore, **16i** demonstrated distinct properties of anti-fibrotic and calcific effects. In summary, compound **16i** shows great potential as a valuable preclinical candidate for drug therapy of hepatic fibrosis.

4. Experimental section

4.1. General materials and methods

All used materials and solvents were obtained from the commercial provider without further purification. All reactions were monitored by thin layer chromatography (TLC), and the related compounds were separated by column chromatographyon on a silica gel (200–300 mesh). Mass spectra (MS) were recorded on a QSTAR XL Hybrid MS/MS mass spectrometer. ^{1}H NMR and ^{13}C NMR spectra were recorded on Bruker AV-300 spectrometer with $CDCl_3$ or DMSO-d_6 as the solvents. The chemical shifts were signified in ppm (δ) relative to the internal standard tetramethylsilane (TMS), and coupling constants were signified in hertz (Hz). The purity of the test compounds was analyzed by HPLC，and that for all compounds was ≥95%.

4.1.1. The synthetic methods for compounds 2–14

*4.1.1.1. 3-tert-Butyldimethylsilyloxy benzaldehyde (**2a**).* To a stirred solution of 3-hydroxybenzaldehyde (10.0 g, 0.082 mol) in CH_2Cl_2 (150 mL) was added TBSCl (14.8 g, 0.1 mol) and Imidazole (6.7 g, 0.10 mol). The reaction mixture was stirred at room temperature for 2 h and then H_2O (100 mL) was added to separate. The aqueous phase was further extracted with CH_2Cl_2 (2 × 50 mL). Merged organic phases was washed with brine, dried with Na_2SO_4, and concentrated to give compound ***2a*** as oil. (18.1 g, 94.2% yield).

Compounds **2b** was synthesized by a route similar to that for the synthesis of compound **2a**.

*4.1.1.2. 4-tert-Butyldimethylsilyloxy benzaldehyde (**2b**).* A white oil, 95.7% yield.

*4.1.1.3. 4-Methylphthalic acid (**4**).* 4-methyl phthalic anhydride (50.0 g, 0.31 mol) was dissolved in 250 ml methanol and slowly added with NaOH solution (25 mL, 0.6 M) under stirring condition. The solution was stirred at room temperature for 1 h, and the methanol was removed under vacuum, pH was adjusted to about 2 with 1.0 M hydrochloric acid. Add little water to the treated solution, the aqueous phase was extracted with ethyl acetate (3 × 100 mL), and the organic layer was concentrated to obtain white solid compound **4**. (54.2 g, 97.8% yield).

*4.1.1.4. Ethyl-4-methyl phthalate (**5**).* 4-Methylphthalic acid (50.0 g, 0.28 mol) was dissolved in 300 mL Ethanol, and 45 mL concentrated sulfuric acid was added slowly in the stirring state. After addition, the reaction temperature was raised to 90 °C. After 10 h, the reaction was also cooled to room temperature and dried，pH was adjusted to about 6 with 2.5 M NaOH solution. Add little water to the treated solution, the aqueous phase was extracted with ethyl acetate (3 × 100 mL), and the organic layer was concentrated to obtain white solid compound **5**. (59.8 g, 91.2% yield).

*4.1.1.5. Diethyl-4-(bromomethyl) phthalate (**6**).* To a stirred solution of compound **5** (25 g, 0.12 mol) in CCl_4 (250 mL) was added *N*-bromosuccinimide (25.64 g, 0.14 mol) and catalytic amount of AIBN (1.74 g,

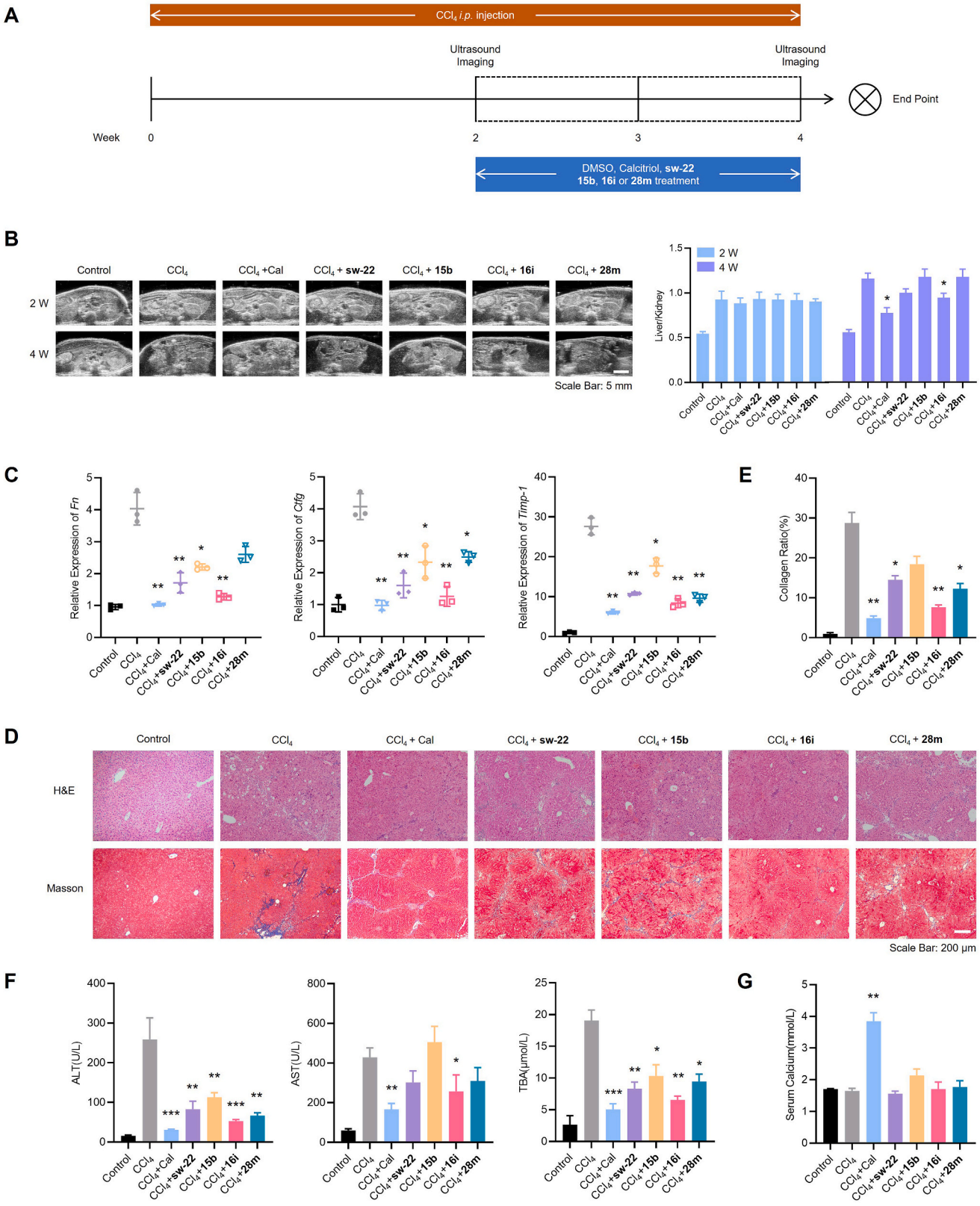

Fig. 7. *In vivo* therapeutic effect of compounds **15b**, **16i,** and **28m** on CCl_4-induced hepatic fibrosis mice. (A) Hepatic fibrosis mice induced by CCl_4 and the treatment regimen with calcipotriol and related compounds. (B) Hepatic fibrosis scores based on the qualitative ultrasound imaging and quantification of the liver and kidney brightness ratio, with both organs on the same section (mean ± SD; $^*P < 0.05$ vs CCl_4-4 w group). (C) Expression levels of *Fn*, *Ctgf,* and *Timp-1* were measured by qPCR (mean ± SD; $^*P < 0.05$ vs CCl_4 group, $^{**}P < 0.01$ vs CCl_4 group). (D) CCl_4-induced hepatic fibrosis lesions were examined by H&E staining (× 100), and the collagen deposition was determined by Masson's Trichrome staining (× 100). (E) The collagen ratio displayed by Masson's Trichrome staining (mean ± SD; $^*P < 0.05$ vs Control group, $^{**}P < 0.01$ vs Control group). (F) Serum levels of ALT, AST, and TBA were determined (mean ± SD; $^*P < 0.05$ vs CCl_4 group, $^{**}P < 0.01$ vs CCl_4 group, $^{***}P < 0.001$ vs CCl_4 group). (G) Serum calcium concentration was determined by a calcium assay kit (mean ± SD; $^{**}P < 0.01$ vs Control group).

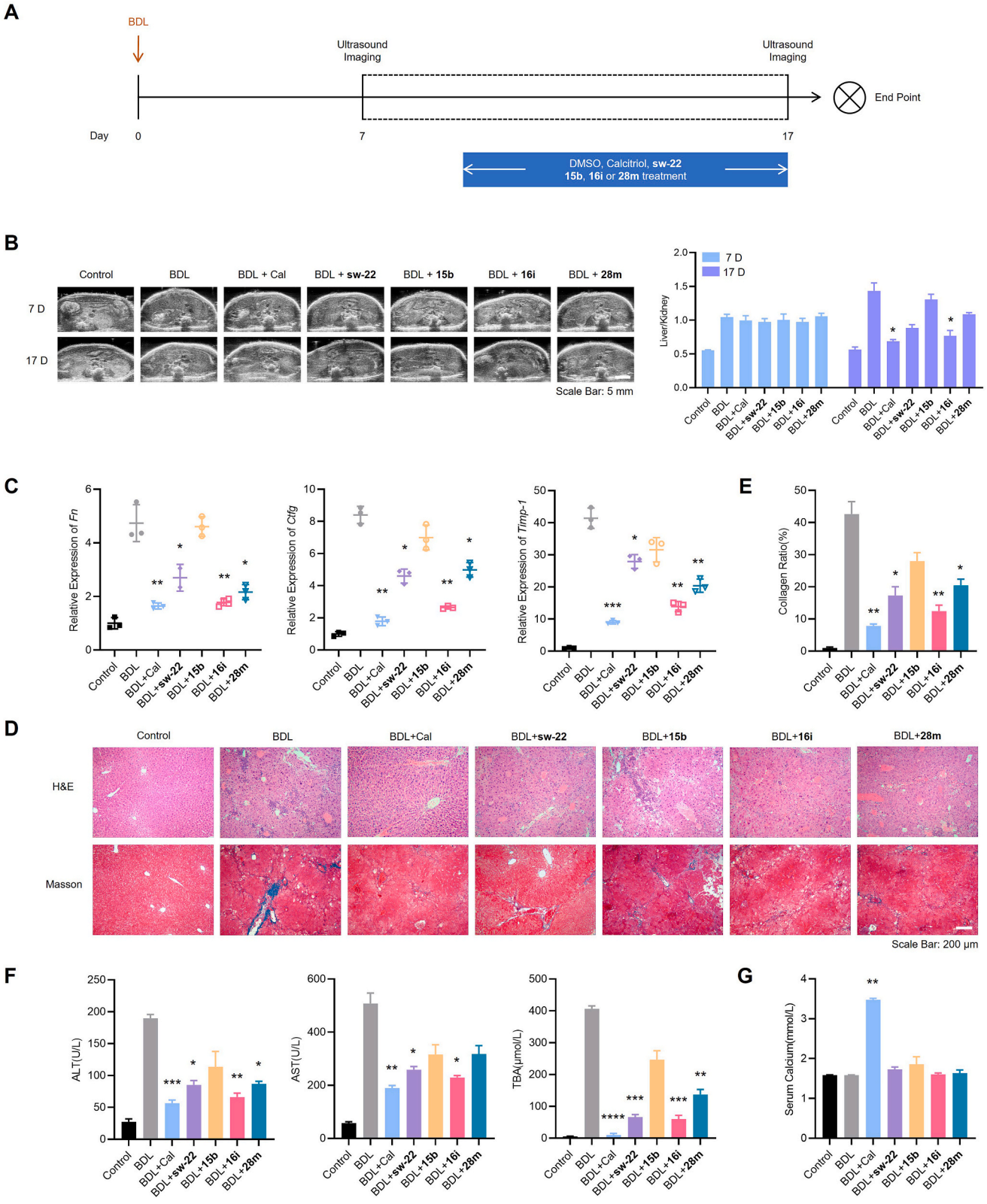

Fig. 8. *In vivo* therapeutic effect of compounds **15b**, **16i**, and **28m** on BDL-induced hepatic fibrosis mice. (A) Hepatic fibrosis mice induced by BDL and the treatment regimen with calcipotriol and related compounds. (B) Hepatic fibrosis scores based on the qualitative ultrasound imaging and quantification of the liver and kidney brightness ratio, with both organs on the same section (mean ± SD; $^{*}P < 0.05$ vs BDL-17 d group). (C) Expression levels of *Fn*, *Ctgf*, and *Timp-1* were measured by qPCR (mean ± SD; $^{*}P < 0.05$ vs BDL group, $^{**}P < 0.01$ vs BDL group, $^{***}P < 0.001$ vs BDL group). (D) BDL-induced hepatic fibrosis lesions were examined by H&E staining (× 100), and the collagen deposition was determined by Masson's Trichrome staining (× 100). (E) The collagen ratio displayed by Masson's Trichrome staining (mean ± SD; $^{*}P < 0.05$ vs Control group, $^{**}P < 0.01$ vs Control group). (F) Serum levels of ALT, AST, and TBA were determined (mean ± SD; $^{*}P < 0.05$ vs BDL group, $^{**}P < 0.01$ vs BDL group, $^{***}P < 0.001$ vs BDL group, $^{****}P < 0.0001$ vs BDL group). (G) Serum calcium concentration was determined by a calcium assay kit (mean ± SD; $^{**}P < 0.01$ vs Control group).

0.011 mol). And then heat up to reflux reaction for 6 h. After the reaction, it was cooled to room temperature, added little water to separate. The aqueous phase was further extracted with CH_2Cl_2 (2 × 50 mL). Merged organic phases was washed with brine and dried over anhydrous Na_2SO_4, filtered and concentrated. The residue was purified by column chromatography with petroleum ether/ethyl acetate (20/1, v/v) to give compound **6** as yellow oil. (21.9 g, 65.7% yield).

*4.1.1.6. Diethyl-(E)-4-(3-((tert-butyldimethylsilyl) oxy) styryl) phthalate **(8a)**.* To a stirred solution of compound **6** (15 g, 0.052 mol) in toluene (200 mL) was slowly added triethylphosphite (50 mL). The reaction solution was refluxed at 150 °C for 12 h. After the reaction, it was cooled to room temperature and concentrated to obtain intermediate compound **7**. The compound **7** (17 g, 0.050 mol) was dissolved in THF (300 mL), and NaH (1.42 g, 0.060 mol) was slowly added under stirring condition. After the reaction at room temperature for 30 min, compound **2** (17.51 g, 0.074 mol) was added to it, and the temperature was raised to 80 °C for reflux 6 h. After the reaction, the reaction solution was cooled to room temperature, and ice water (500 mL) was added to quench the reaction. The aqueous phase was extracted by ethyl acetate (3 × 50 mL), and the combined organic phase was washed with brine, dried with Na_2SO_4, and further purified by column chromatography with petroleum ether/ethyl acetate (20/3, v/v) as the eluent to get compound **8a** as a white oil. (12.8 g, 52.3% yield).

Compounds **8b** was synthesized by a route similar to that for the synthesis of compound **8a**.

*4.1.1.7. Diethyl-(E)-4-(4-((tert-butyldimethylsilyl) oxy) styryl) phthalate **(8b)**.* A white oil, 54.1% yield.

*4.1.1.8. Diethyl-(E)-4-(3-hydroxystyryl) phthalate **(9a)**.* To a stirred solution of compound **8** (10 g, 0.023 mol) in THF (150 mL) was slowly added TBAF (7.4 g, 0.028 mol) THF solution. The mixture was stirred 1 h at room temperature and monitored by TLC. After the reaction, the solvent was evaporated, and water was added to the residue. The resulting solution was extracted with ethyl acetate (3 × 25 mL), and the combined organic phase was washed with brine, dried with Na_2SO_4, and purified by column chromatography with petroleum ether/ethyl acetate (2/1, v/v) as the eluent to get compound **9a** as a white solid. (7.36 g, 98.3% yield).

Compounds **9b** was synthesized by a route similar to that for the synthesis of compound **9a**.

*4.1.1.9. Diethyl-(E)-4-(4-hydroxystyryl) phthalate **(9b)**.* A white solid, 97.1% yield.

*4.1.1.10. (E)-(4-(3-hydroxystyryl)-1,2-phenylene) dimethanol **(10a)**.* To a stirred solution of compound **9** (7 g , 0.022 mmol) in THF (200 mL), was slowly added $LiAlH_4$ (1.72 g, 0.046 mol) at 0 °C. The reaction solution was stirred at room temperature for 4 h. At 0 °C, saturated ammonium chloride (20 mL) was added to quench the reaction, and then ice water (100 mL) was added to stir for 30 min, and aluminum salt was removed by filtration. The organic layer was collected after filter liquor separation, and the aqueous phase was extracted by ethyl acetate (3 × 25 mL). The combined organic phase was washed with brine, dried with Na_2SO_4, and purified by column chromatography with CH_2Cl_2/MeOH (10/1, v/v) as the eluent to get compound **10a** as a white solid. (3.73 g, 70.8% yield).

Compounds **10b** was synthesized by a route similar to that for the synthesis of compound **10a**.

*4.1.1.11. (E)-(4-(4-hydroxystyryl)-1,2-phenylene) dimethanol **(10b)**.* A white solid, 65.5% yield.

*4.1.1.12. (E)-3-(2-(3,3-dimethyl-1,5-dihydrobenzo[e] [1,3] dioxepin-7-yl) vinyl) phenol **(11a)**.* To a stirred solution of compound **10** (3.5 g, 0.014 mol) and 2,2-dimethoxypropane (3.56 g, 0.034 mol) in acetone (50 mL) was slowly added *p*-toluenesulfonic acid (1.18 g, 0.007 mol). The reaction solution stirred at room temperature for 1 h, saturated sodium bicarbonate aqueous solution (10 mL) was added, and then stratified after shock. The Water layer was further extracted with ethyl acetate (3 × 25 mL), and the combined organic phase was washed with brine, dried with Na_2SO_4, and purified by column chromatography with petroleum ether/ethyl acetate (2/1, v/v) as the eluent to get compound **11a** as a white solid. (3.57 g, 88.2% yield).

Compounds **11b** was synthesized by a route similar to that for the synthesis of compound **11a**.

*4.1.1.13. (E)-4-(2-(3,3-dimethyl-1,5-dihydrobenzo[e] **[1,3]** dioxepin-7-yl) vinyl) phenol **(11b)**.* A white solid, 91.7% yield.

*4.1.1.14. Methyl-(E)-3-(3-(2-(3,3-dimethyl-1,5-dihydrobenzo[e] **[1,3]** dioxepin-7-yl) vinyl) phenoxy) propanoate **(12a)**.* To a stirred solution of compound **11** (0.5 g, 1.69 mmol) in DMF (30 mL), NaH (60.73 mg, 2.53 mmol) was added portionwise at 0 °C. After stirring for 30 min, methyl-3-bromopropanoate (0.34 g, 2.02 mmol) was added. The reaction mixture was stirred at room temperature for 12 h and then H_2O (200 mL) was added to quench the reaction. The aqueous phase was extracted by ethyl acetate (3 × 25 mL), and the combined organic phase was washed with brine, dried with Na_2SO_4, and further purified by column chromatography with petroleum ether/ethyl acetate (8/1, v/v) as the eluent to get compound **12a** as a white oil. (0.45 g, 69.7% yield).

Compounds **12b-12e** were synthesized by a route similar to that for the synthesis of compound **12a**.

*4.1.1.15. Methyl-(E)-4-(3-(2-(3,3-dimethyl-1,5-dihydrobenzo[e] **[1,3]** dioxepin-7-yl) vinyl) phenoxy) butanoate **(12b)**.* A white oil, 52.7% yield.

*4.1.1.16. Methyl-(E)-5-(3-(2-(3,3-dimethyl-1,5-dihydrobenzo[e] **[1,3]** dioxepin-7-yl) vinyl) phenoxy) pentanoate **(12c)**.* A white oil, 73.6% yield.

*4.1.1.17. Methyl-(E)-5-(4-(2-(3,3-dimethyl-1,5-dihydrobenzo[e] **[1,3]** dioxepin-7-yl) vinyl) phenoxy) pentanoate **(12d)**.* A white oil, 75.4% yield.

*4.1.1.18. Methyl-(E)-6-(3-(2-(3,3-dimethyl-1,5-dihydrobenzo[e] **[1,3]** dioxepin-7-yl) vinyl) phenoxy) hexanoate **(12e)**.* A white oil, 65.3% yield.

*4.1.1.19. (E)-3-(3-(2-(3,3-dimethyl-1,5-dihydrobenzo[e] **[1,3]** dioxepin-7-yl) vinyl) phenoxy)-N, N-diethylpropan-1-amine **(13a)**.* Compounds **11a** (0.3 g, 1.01 mmol), 3-(diethylamino)propan-1-ol (0.17 g, 1.32 mmol) and PPh_3 (0.4 g, 1.52 mmol) were dissolved in THF (50 mL) , and the reaction system was protected by N_2 atmosphere and pre-cooled under ice bath. DEAD (0.26g, 1.52 mmol) was slowly added at 0 °C, stirred for 30 min, and then transferred to room temperature with N_2 atmosphere for agitation overnight. The complete consumption of starting materials was monitored by TLC. Appropriate amount of water was added to separate the organic layer, and the aqueous phase was extracted with ethyl acetate (3 × 10 mL). The organic phase was combined, washed with brine, dried with Na_2SO_4, and the intermediate compound **13a** was obtained as a white oil by column chromatography (CH_2Cl_2/MeOH: 20/1, v/v) after concentration. (0.20 g, 48.7% yield).

Compounds **13b-13h** were synthesized by a route similar to that for the synthesis of compound **13a**.

*4.1.1.20. (E)-3-(4-(2-(3,3-dimethyl-1,5-dihydrobenzo[e] **[1,3]** dioxepin-7-yl) vinyl) phenoxy)-N, N-diethylpropan-1-amine **(13b)**.* A white solid, 56.4% yield.

4.1.1.21. (E)-4-(3-(3-(2-(3,3-dimethyl-1,5-dihydrobenzo[e] ***[1,3]*** *dioxe pin-7-yl) vinyl) phenoxy) propyl) morpholine (**13c**).* A white oil, 40.9% yield.

*4.1.1.22. (E)-4-(3-(4-(2-(3,3-dimethyl-1,5-dihydrobenzo[e] [1,3] dioxe pin-7-yl) vinyl) phenoxy) propyl) morpholine (**13d**).* A white solid, 46.5% yield.

*4.1.1.23. (E)-3,3-dimethyl-7-(3-(4,4,4-trifluorobutoxy) styryl)-1,5-dihydrobenzo[e] [1,3] dioxepine (**13e**).* A white solid, 62.9% yield.

*4.1.1.24. (E)-3,3-dimethyl-7-(4-(4,4,4-trifluorobutoxy) styryl)-1,5-dihyd robenzo[e] [1,3] dioxepine (**13f**).* A white solid, 68.8% yield.

*4.1.1.25. (E)-1-(3-(4-(2-(3,3-dimethyl-1,5-dihydrobenzo[e] [1,3] dioxe-pin -7-yl) vinyl) phenoxy) propyl)-4-methylpiperazine (**13g**).* A white oil, 31.7% yield.

*4.1.1.26. (E)-5-(3-(2-(3,3-dimethyl-1,5-dihydrobenzo[e] [1,3] dioxepin-7-yl) vinyl) phenoxy) pentan-2-one (**13h**).* A white oil, 65.3% yield.

*4.1.1.27. (E)-4-(3-(2-(3,3-dimethyl-1,5-dihydrobenzo[e] [1,3] dioxepin-7-yl) vinyl) phenoxy) butanoic acid (**13i**).* To a stirred solution of compound **12b** (0.5 g, 1.26 mmol) in MeOH (20 mL) was slowly added 1 M NaOH solution (1.5 mL). The mixture solution was stirred at room temperature for 1 h, and the methanol was removed under vacuum, pH was adjusted to about 2 with 1.0 M HCl. Add little water to the solution, the aqueous phase was extracted with ethyl acetate (3 × 10 mL), and the organic layer was concentrated to obtain white solid compound **13i**. (0.38 g, 78.8% yield).

*4.1.1.28. (E)-4-(3-(2-(3,3-dimethyl-1,5-dihydrobenzo[e] [1,3] dioxepin-7-yl) vinyl) phenoxy) butan-1-ol (**14a**).* To a stirred solution of compound **12b** (0.5 g, 1.26 mmol) in THF (50 mL) was slowly added $LiAlH_4$ (34.46 mg, 1 mmol). The mixture solution was stirred at room temperature for 2 h, and then saturated ammonium chloride solution (10 mL) was added to quench the reaction. Subsequently, ice water (30 mL) was added to stir for 30 min, and aluminum salt was removed by filtration. The filter liquor was extracted by ethyl acetate (3 × 10 mL) and the combined organic phase was washed with brine, dried with Na_2SO_4, and purified by column chromatography with petroleum ether/ethyl acetate (20/3, v/v) as the eluent to get compound **14a** as a white oil. (0.14 g, 51.3% yield).

Compounds **14b-14c** were synthesized by a route similar to that for the synthesis of compound **14a**.

*4.1.1.29. (E)-5-(4-(2-(3,3-dimethyl-1,5-dihydrobenzo[e] [1,3] dioxepin-7-yl) vinyl) phenoxy) pentan-1-ol (**14b**).* A white oil, 57.1% yield.

*4.1.1.30. (E)-5-(3-(2-(3,3-dimethyl-1,5-dihydrobenzo[e] [1,3] dioxepin-7-yl) vinyl) phenoxy) pentan-2-ol (**14c**).* A white oil, 46.4% yield.

*4.1.1.31. (E)-5-(3-(2-(3,3-dimethyl-1,5-dihydrobenzo[e] [1,3] dioxepin-7-yl) vinyl) phenoxy)-2-methylpentan-2-ol (**14d**).* To a stirred solution of compound **12b** (0.3 g, 0.76 mmol) in THF (50 mL) was slowly added CH_3MgBr (0.23 g, 1.89 mmol) -THF solution at N_2 atmosphere. The mixture solution was stirred at room temperature for 6 h, and then saturated ammonium chloride solution (10 mL) was added to quench the reaction. Subsequently, H_2O (100 mL) was added and the aqueous phase was extracted with ethyl acetate (3 × 10 mL). The organic phase was combined, washed with brine, dried with Na_2SO_4, and purified by column chromatography with petroleum ether/ethyl acetate (20/3, v/v) as the eluent to get compound **14d** as a white oil. (0.23 g, 76.7% yield).

Compounds **14e-14j** were synthesized by a route similar to that for the synthesis of compound **14d**.

*4.1.1.32. (E)-1-(3-(2-(3,3-dimethyl-1,5-dihydrobenzo[e] [1,3] dioxepin-7-yl) vinyl) phenoxy)-3-ethylpentan-3-ol (**14e**).* A white oil, 68.3% yield.

*4.1.1.33. (E)-6-(3-(2-(3,3-dimethyl-1,5-dihydrobenzo[e] [1,3] dioxepin-7-yl) vinyl) phenoxy)-3-ethylhexan-3-ol (**14f**).* A white oil, 75.6% yield.

*4.1.1.34. (E)-4-(3-(3-(2-(3,3-dimethyl-1,5-dihydrobenzo[e] [1,3] dioxe pin-7-yl) vinyl) phenoxy) propyl) hepta-1,6-dien-4-ol (**14g**).* A white oil, 64.7% yield.

*4.1.1.35. (E)-7-(3-(2-(3,3-dimethyl-1,5-dihydrobenzo[e] [1,3] dioxepin-7-yl) vinyl) phenoxy)-3-ethylheptan-3-ol (**14h**).* A white oil, 77.8% yield.

*4.1.1.36. (E)-7-(4-(2-(3,3-dimethyl-1,5-dihydrobenzo[e] [1,3] dioxepin-7-yl) vinyl) phenoxy)-3-ethylheptan-3-ol (**14i**).* A white oil, 69.5% yield.

*4.1.1.37. (E)-8-(3-(2-(3,3-dimethyl-1,5-dihydrobenzo[e] [1,3] dioxepin-7-yl) vinyl) phenoxy)-3-ethyloctan-3-ol (**14j**).* A white oil, 65.5% yield.

*4.1.2. The synthetic methods for target compounds **15a-l** and **16a-i***

*4.1.2.1. (E)-(4-(3-((3-ethyl-3-hydroxypentyl) oxy) styryl)-1,2-phenylene) dimethanol (**15a**).* To a stirred solution of compound **14e** (0.15 g, 0.36 mmol) in THF (30 mL) was slowly added *p*-Toluenesulfonic acid monohydrate (69.21 mg, 0.40 mmol). After stirred at room temperature for 30 min, H_2O (50 mL) was added to the mixture solution and the aqueous phase was extracted with ethyl acetate (3 × 10 mL). The organic phase was combined, washed with brine, dried with Na_2SO_4, and purified by column chromatography with CH_2Cl_2/MeOH (40/1, v/v) as the eluent to get compound **15a** as a white solid. (87 mg, 64.3% yield).

Compounds **15b-15l** and **16a-i** were synthesized by a route similar to that for the synthesis of compound **15a**.

*4.1.2.2. (E)-(4-(3-((4-ethyl-4-hydroxyhexyl) oxy) styryl)-1,2-phenylene) dimethanol (**15b**).* A white solid, 67.9% yield.

*4.1.2.3. (E)-(4-(3-((5-ethyl-5-hydroxyheptyl) oxy) styryl)-1,2-phenylene) dimethanol (**15c**).* A white solid, 64.8% yield.

*4.1.2.4. (E)-(4-(3-((6-ethyl-6-hydroxyoctyl) oxy) styryl)-1,2-phenylene) dimethanol (**15d**).* A white solid, 65.5% yield.

*4.1.2.5. (E)-(4-(3-(4-hydroxybutoxy) styryl)-1,2-phenylene) dimethanol (**15e**).* A white solid, 58.6% yield.

*4.1.2.6. (E)-(4-(3-((4-hydroxy-4-methylpentyl) oxy) styryl)-1,2-pheny lene) dimethanol (**15f**).* A white solid, 62.7% yield.

*4.1.2.7. (E)-(4-(3-((4-allyl-4-hydroxyhept-6-en-1-yl) oxy) styryl)-1,2- phenylene) dimethanol (**15g**).* A white solid, 68.9% yield.

*4.1.2.8. (E)-(4-(3-(4-hydroxy-4,4-diphenylbutoxy) styryl)-1,2-phenylene) dimethanol (**15h**).* A white solid, 60.3% yield.

*4.1.2.9. (E)-(4-(3-((4-hydroxypentyl) oxy) styryl)-1,2-phenylene) dimethanol (**15i**).* A white solid, 56.5% yield.

*4.1.2.10. (E)-(4-(3-((5-hydroxypentyl) oxy) styryl)-1,2-phenylene) dimethanol (**15j**).* A white solid, 57.8% yield.

*4.1.2.11. (E)-(4-(4-((5-ethyl-5-hydroxyheptyl) oxy) styryl)-1,2-phenylene) dimethanol (**15k**).* A white solid, 67.7% yield.

*4.1.2.12. (E)-(4-(4-((5-hydroxypentyl) oxy) styryl)-1,2-phenylene) dimethanol (**15l**).* A white solid, 57.8% yield.

*4.1.2.13. (E)-(4-(3-(3-(diethylamino) propoxy) styryl)-1,2-phenylene) dime thanol (**16a**).* A white solid, 60.5% yield.

*4.1.2.14. (E)-(4-(3-(3-morpholinopropoxy) styryl)-1,2-phenylene) dimethanol (**16b**).* A white solid, 62.3% yield.

*4.1.2.15. (E)-(4-(3-(4,4,4-trifluorobutoxy) styryl)-1,2-phenylene) dimethanol (**16c**).* A white solid, 58.8% yield.

*4.1.2.16. Methyl-(E)-4-(3-(3,4-bis(hydroxymethyl) styryl) phenoxy) butanoate (**16d**).* A white solid, 68.4% yield.

*4.1.2.17. (E)-4-(3-(3,4-bis(hydroxymethyl) styryl) phenoxy) butanoic acid (**16e**).* A white solid, 55.6% yield.

*4.1.2.18. (E)-(4-(4-(3-(diethylamino) propoxy) styryl)-1,2-phenylene) dimethanol (**16f**).* A white solid, 61.4% yield.

*4.1.2.19. (E)-(4-(4-(3-morpholinopropoxy) styryl)-1,2-phenylene) dimethanol (**16g**).* A white solid, 60.5% yield.

*4.1.2.20. (E)-(4-(4-(3-(4-methylpiperazin-1-yl) propoxy) styryl)-1,2-phenylene) dimethanol (**16h**).* A white solid, 58.4% yield.

*4.1.2.21. (E)-(4-(4-(4,4,4-trifluorobutoxy) styryl)-1,2-phenylene) dimethanol (**16i**).* A white solid, 68.9% yield.

*4.1.3. The synthetic methods for target compounds **17a-h***

*4.1.3.1. (4-(3-(4-hydroxybutoxy) phenethyl)-1,2-phenylene) dimethanol (**17a**).* To a stirred solution of compound **15e** (0.10 g, 0.31 mmol) and CH_3COONa (0.25 g, 3.04 mmol) in EtOH (50 mL) was slowly added 4-Methylbenzenesulfonhydrazide (0.57 g, 3.04 mmol). Then the reaction system temperature was raised to 90 °C, reflux for 12 h. The complete consumption of starting materials was monitored by TLC. Appropriate amount of water was added to separate the organic layer, and the aqueous phase was extracted with ethyl acetate (3 × 25 mL). The organic phase was combined, washed with brine, dried with Na_2SO_4, and the compound **17a** was obtained as a white solid after concentration. (97 mg, 96.8% yield).

Compounds **17b-17h** were synthesized by a route similar to that for the synthesis of compound **17a**.

*4.1.3.2. (4-(3-((4-hydroxy-4-methylpentyl) oxy) phenethyl)-1,2-phenylene) dimethanol (**17b**).* A white solid, 90.4% yield.

*4.1.3.3. (4-(3-((4-ethyl-4-hydroxyhexyl) oxy) phenethyl)-1,2-phenylene) dimethanol (**17c**).* A white solid, 94.5% yield.

*4.1.3.4. (4-(3-((4-allyl-4-hydroxyhept-6-en-1-yl) oxy) phenethyl)-1,2-phenylene) dimethanol (**17d**).* A white solid, 87.6% yield.

*4.1.3.5. (4-(4-((5-hydroxypentyl) oxy) phenethyl)-1,2-phenylene) dimethanol (**17e**).* A white solid, 94.4% yield.

*4.1.3.6. (4-(4-((5-hydroxy-5-methylhexyl) oxy) phenethyl)-1,2-phenylene) dimethanol (**17f**).* A white solid, 89.6% yield.

*4.1.3.7. (4-(4-((5-ethyl-5-hydroxyheptyl) oxy) phenethyl)-1,2-phenylene) dimethanol (**17g**).* A white solid, 95.7% yield.

*4.1.3.8. (4-(4-((5-allyl-5-hydroxyoct-7-en-1-yl) oxy) phenethyl)-1,2-phenylene) dimethanol (**17h**).* A white solid, 91.6% yield.

*4.1.4. The synthetic methods for compounds **18**–**27***

*4.1.4.1. (3-((tert-butyldimethylsilyl) oxy) phenyl) methanol (**18a**).* To a stirred solution of compound **2** (10 g, 42.30 mmol) in THF (300 mL) was slowly added $LiAlH_4$ (1.93 g, 50.76 mmol) at 0 °C. After stirred for 6 h, saturated ammonium chloride solution (25 mL) was added to quench the reaction. Subsequently, ice water (200 mL) was added to stir for 30 min, and aluminum salt was removed by filtration. The filter liquor was extracted by ethyl acetate (3 × 50 mL) and the combined organic phase was washed with brine, dried with Na_2SO_4, and compound **18a** was obtained as a white oil after concentration. (7.67 g, 76.0% yield).

*4.1.4.2. 1-(3-((tert-butyldimethylsilyl) oxy) phenyl) ethan-1-ol (**18b**).* To a stirred solution of compound **2** (10 g, 42.30 mmol) in THF (300 mL) was slowly dropped CH_3MgBr (6.05 g, 50.76 mmol) -THF solution at N_2 atmosphere. The mixture solution was stirred for 4 h[quench the reaction. H_2O (200 mL) was added and the aqueous phase was extracted with ethyl acetate (3 × 50 mL). The organic phase was combined, washed with brine, dried with Na_2SO_4, compound **18b** was obtained as a white oil after concentration. (7.86 g, 73.6% yield).

Compounds **18c-18f** were synthesized by a route similar to that for the synthesis of compound **18b**.

*4.1.4.3. 1-(3-((tert-butyldimethylsilyl) oxy) phenyl) propan-1-ol (**18c**).* A white oil, 65.7% yield.

*4.1.4.4. 1-(3-((tert-butyldimethylsilyl) oxy) phenyl) butan-1-ol (**18d**).* A white oil, 57.5% yield.

*4.1.4.5. 1-(3-((tert-butyldimethylsilyl) oxy) phenyl)-2-methylpropan-1-ol (**18e**).* A white oil, 33.2% yield.

*4.1.4.6. 1-(3-((tert-butyldimethylsilyl) oxy) phenyl) pentan-1-ol (**18f**).* A white oil, 40.3% yield.

*4.1.4.7. Diethyl-4-hydroxyphthalate (**20**).* The same method as that of compound **5** was used, and the starting materials were 4-hydroxyphthalic acid. A yellow oil. (28.2 g, 86.2% yield).

*4.1.4.8. Diethyl-4-((3-((tert-butyldimethylsilyl) oxy) benzyl) oxy) phthalate (**21a**).* Compounds **20** (10 g, 41.97 mmol), compound 18a (13.01 g, 54.57 mmol) and PPh_3 (16.51 g, 62.96 mmol) were dissolved in THF (500 mL) , and the reaction system was protected by N_2 atmosphere and pre-cooled under ice bath. DEAD (0.26g, 1.52 mmol) was slowly added at 0 °C, stirred for 30 min, and then transferred to room temperature with N_2 atmosphere for agitation overnight. The complete consumption of starting materials was monitored by TLC. Appropriate amount of water was added to separate the organic layer, and the aqueous phase was extracted with ethyl acetate (3 × 50 mL). The organic phase was combined, washed with brine, dried with Na_2SO_4, and the intermediate compound **21a** was obtained as a white oil by column chromatography (petroleum ether/ethyl acetate: 20/1, v/v) after concentration. (10.35 g, 53.7% yield).

Compounds **21b-21f** were synthesized by a route similar to that for the synthesis of compound **21a**.

*4.1.4.9. Diethyl-4-(1-(3-((tert-butyldimethylsilyl) oxy) phenyl) ethoxy) phthalate (**21b**).* A white oil, 49.7% yield.

*4.1.4.10. Diethyl-4-(1-(3-((tert-butyldimethylsilyl) oxy) phenyl) propoxy) phthalate (**21c**).* A white oil, 45.2% yield.

*4.1.4.11. Diethyl-4-(1-(3-((tert-butyldimethylsilyl) oxy) phenyl) butoxy) phthalate (**21d**).* A white oil, 37.4% yield.

*4.1.4.12. Diethyl-4-(1-(3-((tert-butyldimethylsilyl) oxy) phenyl)-2-methyl propoxy) phthalate (**21e**).* A white oil, 23.3% yield.

*4.1.4.13. Diethyl-4-((1-(3-((tert-butyldimethylsilyl) oxy) phenyl) pentyl) oxy) phthalate (**21f**).* A white oil, 28.6% yield.

The same method as that of compound **9** was used, and just the starting materials **9** was respectively substituted with compound **21a**, **21b**, **21c**, **21d**, **21e**, **21f**.

*4.1.4.14. Diethyl-4-((3-hydroxybenzyl) oxy) phthalate (**22a**).* A white oil, 94.5% yield.

*4.1.4.15. Diethyl-4-(1-(3-hydroxyphenyl) ethoxy) phthalate (**22b**).* A white oil, 95.2% yield.

*4.1.4.16. Diethyl-4-(1-(3-hydroxyphenyl) propoxy) phthalate (**22c**).* A white oil, 94% yield.

*4.1.4.17. Diethyl-4-(1-(3-hydroxyphenyl) butoxy) phthalate (**22d**).* A white oil, 93.8% yield.

*4.1.4.18. Diethyl-4-(1-(3-hydroxyphenyl)-2-methylpropoxy) phthalate (**22e**).* A white oil, 93.1% yield.

*4.1.4.19. Diethyl-4-((1-(3-hydroxyphenyl) pentyl) oxy) phthalate (**22f**).* A white oil, 94.7% yield.

The same method as that of compound **10** was used, and just the starting materials **10** was respectively substituted with compound **22a**, **22b**, **22c**, **22d**, **22e**, **22f**.

*4.1.4.20. (4-((3-hydroxybenzyl) oxy)-1,2-phenylene) dimethanol (**23a**).* A white solid, 68.6% yield.

*4.1.4.21. (4-((3-hydroxybenzyl) oxy)-1,2-phenylene) dimethanol (**23b**).* A white solid, 67.8% yield.

*4.1.4.22. (4-((3-hydroxybenzyl) oxy)-1,2-phenylene) dimethanol (**23c**).* A white solid, 64% yield.

*4.1.4.23. (4-((3-hydroxybenzyl) oxy)-1,2-phenylene) dimethanol (**23d**).* A white solid, 65.9% yield.

*4.1.4.24. (4-((3-hydroxybenzyl) oxy)-1,2-phenylene) dimethanol (**23e**).* A white solid, 62.2% yield.

*4.1.4.25. (4-((3-hydroxybenzyl) oxy)-1,2-phenylene) dimethanol (**23f**).* A white solid, 63.8% yield.

The same method as that of compound **11** was used, and just the starting materials **10** was respectively substituted with compound **23a**, **23b**, **23c**, **23d**, **23e**, **23f**.

*4.1.4.26. 3-(((3,3-dimethyl-1,5-dihydrobenzo[e] [1,3] dioxepin-7-yl) oxy) methyl) phenol (**24a**).* A white solid, 89.6% yield.

*4.1.4.27. 3-(1-((3,3-dimethyl-1,5-dihydrobenzo[e] [1,3] dioxepin-7-yl) oxy) ethyl) phenol (**24b**).* A white solid, 88.5% yield.

*4.1.4.28. 3-(1-((3,3-dimethyl-1,5-dihydrobenzo[e] [1,3] dioxepin-7-yl) oxy) propyl) phenol (**24c**).* A white solid, 88.2% yield.

*4.1.4.29. 3-(1-((3,3-dimethyl-1,5-dihydrobenzo[e] [1,3] dioxepin-7-yl) oxy) butyl) phenol (**24d**).* A white solid, 87% yield.

*4.1.4.30. 3-(1-((3,3-dimethyl-1,5-dihydrobenzo[e] [1,3] dioxepin-7-yl) oxy)-2-methylpropyl) phenol (**24e**).* A white solid, 85.5% yield.

*4.1.4.31. 3-(1-((3,3-dimethyl-1,5-dihydrobenzo[e] [1,3] dioxepin-7-yl) oxy) pentyl) phenol (**24f**).* A white solid, 86.7% yield.

The same method as that of compound **12a** was used, and just the starting materials **11** was respectively substituted with compound **24a**, **24b**, **24c**, **24d**, **24e**, **24f**.

*4.1.4.32. Methyl-4-(3-(((3,3-dimethyl-1,5-dihydrobenzo[e] [1,3] dioxepin-7-yl) oxy) methyl) phenoxy) butanoate (**25a**).* A white solid, 65.2% yield.

*4.1.4.33. Methyl-4-(3-(1-((3,3-dimethyl-1,5-dihydrobenzo[e] [1,3] dioxe pin-7-yl) oxy) ethyl) phenoxy) butanoate (**25b**).* A white solid, 60.3% yield.

*4.1.4.34. Methyl-4-(3-(1-((3,3-dimethyl-1,5-dihydrobenzo[e] [1,3] dioxe pin-7-yl) oxy) propyl) phenoxy) butanoate (**25c**).* A white solid, 58.8% yield.

*4.1.4.35. Methyl-4-(3-(1-((3,3-dimethyl-1,5-dihydrobenzo[e] [1,3] dioxe pin-7-yl) oxy) butyl) phenoxy) butanoate (**25d**).* A white solid, 57.4% yield.

*4.1.4.36. Methyl-4-(3-(1-((3,3-dimethyl-1,5-dihydrobenzo[e] [1,3] dioxe pin-7-yl) oxy)-2-methylpropyl) phenoxy) butanoate (**25e**).* A white solid, 53.6% yield.

*4.1.4.37. Methyl-4-(3-(1-((3,3-dimethyl-1,5-dihydrobenzo[e] [1,3] dioxe pin-7-yl) oxy) pentyl) phenoxy) butanoate (**25f**).* A white solid, 60.7% yield.

*4.1.4.38. 3-(3-(((3,3-dimethyl-1,5-dihydrobenzo[e] [1,3] dioxepin-7-yl) oxy) methyl) phenoxy)-N, N-diethylpropan-1-amine (**26a**).* The same method as that of compound 13a was used, and just the starting materials 11a was substituted with compound **24a**. A white oli. (0.22 g, 42.6% yield).

*4.1.4.39. 4-(3-(((3,3-dimethyl-1,5-dihydrobenzo[e] [1,3] dioxepin-7-yl) oxy) methyl) phenoxy) butanoic acid (**26b**).* The same method as that of compound **13f** was used, and just the starting materials **12b** was substituted with compound **25a**. A white solid. (0.36 g, 82.8% yield).

*4.1.4.40. 4-(3-(((3,3-dimethyl-1,5-dihydrobenzo[e] [1,3] dioxepin-7-yl) oxy) methyl) phenoxy)-N, N-diethylbutanamide (**26c**).* To a stirred solution of compound **26b** (0.3 g, 0.77 mmol) in CH_2Cl_2 (30 mL) was slowly added EDCI (0.18 g, 1.16 mmol) and HOBT (0.16 g, 1.16 mmol) at room temperature. After stirred for 2 h, diethylamine (73.81 mg, 1.01 mmol) and Et_3N (0.16 g, 0.55 mmol) was added to the mixture solution. After the reaction, H_2O (50 mL) was added and the aqueous phase was extracted with CH_2Cl_2 (3 × 10 mL). The organic phase was combined, washed with brine, dried with Na_2SO_4, and compound **26c** was obtained as a white oil by column chromatography (petroleum/ether ethyl acetate: 5/1, v/v) after concentration. (0.22 g, 63.5% yield).

The same method as that of compound **26c** was used, and just the starting materials diethylamine was respectively substituted with piperidine, morpholine, 1-methylpiperazine.

*4.1.4.41. 4-(3-(((3,3-dimethyl-1,5-dihydrobenzo[e] [1,3] dioxepin-7-yl) oxy) methyl) phenoxy)-1-(piperidin-1-yl) butan-1-one (**26d**).* A white oil, 57.2% yield.

*4.1.4.42. 4-(3-(((3,3-dimethyl-1,5-dihydrobenzo[e] [1,3] dioxepin-7-yl) oxy) methyl) phenoxy)-1-morpholinobutan-1-one (**26e**).* A white oil, 60.6% yield.

*4.1.4.43. 4-(3-(((3,3-dimethyl-1,5-dihydrobenzo[e] [1,3] dioxepin-7-yl) oxy) methyl) phenoxy)-1-(4-methylpiperazin-1-yl) butan-1-one (**26f**).* A white oil, 52.5% yield.

Compounds **27a-27p** were synthesized by a route similar to that for the synthesis of compound **14a** and **14d**.

*4.1.4.44. 4-(3-(((3,3-dimethyl-1,5-dihydrobenzo[e] [1,3] dioxepin-7-yl) oxy) methyl) phenoxy) butan-1-ol (**27a**).* A white oil, 57.4% yield.

*4.1.4.45. 5-(3-(((3,3-dimethyl-1,5-dihydrobenzo[e] [1,3] dioxepin-7-yl) oxy) methyl) phenoxy)-2-methylpentan-2-ol (**27b**).* A white oil, 70.5% yield.

*4.1.4.46. 6-(3-(((3,3-dimethyl-1,5-dihydrobenzo[e] [1,3] dioxepin-7-yl) oxy) methyl) phenoxy)-3-ethylhexan-3-ol (**27c**).* A white oil, 63.2% yield.

*4.1.4.47. 4-(3-(3-(((3,3-dimethyl-1,5-dihydrobenzo[e] [1,3] dioxepin-7-yl) oxy) methyl) phenoxy) propyl) hepta-1,6-dien-4-ol (**27d**).* A white oil, 66.7% yield.

*4.1.4.48. 5-(3-(((3,3-dimethyl-1,5-dihydrobenzo[e] [1,3] dioxepin-7-yl) oxy) methyl) phenoxy) pentan-1-ol (**27e**).* A white oil, 53.8% yield.

*4.1.4.49. 6-(3-(((3,3-dimethyl-1,5-dihydrobenzo[e] [1,3] dioxepin-7-yl) oxy) methyl) phenoxy)-2-methylhexan-2-ol (**27f**).* A white oil, 66% yield.

*4.1.4.50. 7-(3-(((3,3-dimethyl-1,5-dihydrobenzo[e] [1,3] dioxepin-7-yl) oxy) methyl) phenoxy)-3-ethylheptan-3-ol (**27g**).* A white oil, 61.2% yield.

*4.1.4.51. 6-(3-(((3,3-dimethyl-1,5-dihydrobenzo[e] [1,3] dioxepin-7-yl) oxy) methyl) phenoxy) hexan-1-ol (**27h**).* A white oil, 68.5% yield.

*4.1.4.52. 7-(3-(((3,3-dimethyl-1,5-dihydrobenzo[e] [1,3] dioxepin-7-yl) oxy) methyl) phenoxy)-2-methylheptan-2-ol (**27i**).* A white oil, 63% yield.

*4.1.4.53. 8-(3-(((3,3-dimethyl-1,5-dihydrobenzo[e] [1,3] dioxepin-7-yl) oxy) methyl) phenoxy)-3-ethyloctan-3-ol (**27j**).* A white oil, 67.8% yield.

*4.1.4.54. 4-allyl-9-(3-(((3,3-dimethyl-1,5-dihydrobenzo[e] [1,3] dioxepin-7-yl) oxy) methyl) phenoxy) non-1-en-4-ol (**27k**).* A white oil, 65.9% yield.

*4.1.4.55. 6-(3-(1-((3,3-dimethyl-1,5-dihydrobenzo[e] [1,3] dioxepin-7-yl) oxy) ethyl) phenoxy)-3-ethylhexan-3-ol (**27l**).* A white oil, 72.6% yield.

*4.1.4.56. 6-(3-(1-((3,3-dimethyl-1,5-dihydrobenzo[e] [1,3] dioxepin-7-yl) oxy) propyl) phenoxy)-3-ethylhexan-3-ol (**27m**).* A white oil, 68.5% yield.

*4.1.4.57. 6-(3-(1-((3,3-dimethyl-1,5-dihydrobenzo[e] [1,3] dioxepin-7-yl) oxy) butyl) phenoxy)-3-ethylhexan-3-ol (**27n**).* A white oil, 65.1% yield.

*4.1.4.58. 6-(3-(1-((3,3-dimethyl-1,5-dihydrobenzo[e] [1,3] dioxepin-7-yl) oxy)-2-methylpropyl) phenoxy)-3-ethylhexan-3-ol (**27o**).* A white oil, 63.6% yield.

*4.1.4.59. 6-(3-(1-((3,3-dimethyl-1,5-dihydrobenzo[e] [1,3] dioxepin-7-yl) oxy) pentyl) phenoxy)-3-ethylhexan-3-ol (**27p**).* A white oil, 60.8% yield.

*4.1.5. The synthetic methods for target compounds **28a-p** and **29a-i***

Compounds **28a-p** and **29a-i** were synthesized by a route similar to that for the synthesis of compound **15a**.

*4.1.5.1. (4-((3-(4-hydroxybutoxy) benzyl) oxy)-1,2-phenylene) dimethanol (**28a**).* A white oil, 65.6% yield.

*4.1.5.2. (4-((3-((4-hydroxy-4-methylpentyl) oxy) benzyl) oxy)-1,2-phenylene) dimethanol (**28b**).* A white oil, 71.4% yield.

*4.1.5.3. (4-((3-((4-ethyl-4-hydroxyhexyl) oxy) benzyl) oxy)-1,2-phenylene) dimethanol (**28c**).* A white oil, 70.5% yield.

*4.1.5.4. (4-((3-((4-allyl-4-hydroxyhept-6-en-1-yl) oxy) benzyl) oxy)-1,2-phenylene) dimethanol (**28d**).* A white oil, 68.9% yield.

*4.1.5.5. (4-((3-((5-hydroxypentyl) oxy) benzyl) oxy)-1,2-phenylene) dimethanol (**28e**).* A white oil,72.2% yield.

*4.1.5.6. (4-((3-((5-hydroxy-5-methylhexyl) oxy) benzyl) oxy)-1,2-phenylene) dimethanol (**28f**).* A white oil, 65.4% yield.

*4.1.5.7. (4-((3-((5-ethyl-5-hydroxyheptyl) oxy) benzyl) oxy)-1,2-phenylene) dimethanol (**28g**).* A white oil, 68.5% yield.

*4.1.5.8. (4-((3-((6-hydroxyhexyl) oxy) benzyl) oxy)-1,2-phenylene) dimethanol (**28h**).* A white oil, 67.5% yield.

*4.1.5.9. (4-((3-((6-hydroxy-6-methylheptyl) oxy) benzyl) oxy)-1,2-phenylene) dimethanol (**28i**).* A white oil, 69.3% yield.

*4.1.5.10. (4-((3-((6-ethyl-6-hydroxyoctyl) oxy) benzyl) oxy)-1,2-phenylene) dimethanol (**28j**).* A white oil, 67.5% yield.

*4.1.5.11. (4-((3-((6-allyl-6-hydroxynon-8-en-1-yl) oxy) benzyl) oxy)-1,2-phenylene) dimethanol (**28k**).* A white oil, 58.6% yield.

*4.1.5.12. (4-(1-(3-((4-ethyl-4-hydroxyhexyl) oxy) phenyl) ethoxy)-1,2-phenylene) dimethanol (**28l**).* A white oil, 64.6% yield.

*4.1.5.13. (4-(1-(3-((4-ethyl-4-hydroxyhexyl) oxy) phenyl) propoxy)-1,2-phenylene) dimethanol (**28m**).* A white oil, 70.4% yield.

*4.1.5.14. (4-(1-(3-((4-ethyl-4-hydroxyhexyl) oxy) phenyl) butoxy)-1,2-phenylene) dimethanol (**28n**).* A white oil, 67.8% yield.

*4.1.5.15. (4-(1-(3-((4-ethyl-4-hydroxyhexyl) oxy) phenyl)-2-methyl propoxy)-1,2-phenylene) dimethanol (**28o**).* A white oil, 63.8% yield.

*4.1.5.16. (4-((1-(3-((4-ethyl-4-hydroxyhexyl) oxy) phenyl) pentyl) oxy)-1,2-phenylene) dimethanol (**28p**).* A white oil, 59.6% yield.

*4.1.5.17. (4-((3-(3-(diethylamino) propoxy) benzyl) oxy)-1,2-phenylene) dimethanol (**29a**).* A white oil, 58.8% yield.

*4.1.5.18. Methyl-4-(3-((3,4-bis(hydroxymethyl) phenoxy) methyl) phenoxy) butanoate (**29b**).* A white oil, 73.8% yield.

*4.1.5.19. 4-(3-((3,4-bis(hydroxymethyl) phenoxy) methyl) phenoxy) butanoic acid (**29c**).* A white oil, 66.5% yield.

*4.1.5.20. Methyl-5-(3-((3,4-bis(hydroxymethyl) phenoxy) methyl) phenoxy) pentanoate (**29d**).* A white oil, 70.7% yield.

*4.1.5.21. Methyl-6-(3-((3,4-bis(hydroxymethyl)phenoxy) methyl) phenoxy) hexanoate (**29e**).* A white oil, 71.5% yield.

*4.1.5.22. 4-(3-((3,4-bis(hydroxymethyl) phenoxy) methyl) phenoxy)-N, N-diethylbutanamide (**29f**).* A white oil, 67.5% yield.

*4.1.5.23. 4-(3-((3,4-bis(hydroxymethyl) phenoxy) methyl) phenoxy)-1-(piperidin-1-yl) butan-1-one (**29g**).* A white oil, 64.8% yield.

*4.1.5.24. 4-(3-((3,4-bis(hydroxymethyl) phenoxy) methyl) phenoxy)-1-morpholinobutan-1-one (**29h**).* A white oil, 63.5% yield.

*4.1.5.25. 4-(3-((3,4-bis(hydroxymethyl) phenoxy) methyl) phenoxy)-1-(4-methylpiperazin-1-yl) butan-1-one (**29i**).* A white oil, 68.8% yield.

4.2. VDR binding assay

The assay was performed using PolarScreen™ Vitamin D Receptor Competitor Assay, Red Kit (Thermofisher, Massachusetts, USA), which is a binding assay for determining the IC_{50} values of compounds that bind VDR Full Length. The assay measures the decrease in polarization value accompanying loss of combination of VDR Full Length and Fluormone™ Tracer due to the presence of a competitor. All compounds were supplied in 1% DMSO solution, and were tested for their binding affinity at 1 μM in triplicates. Fluorescence polarization was measured on BioTek Cytation 5 Multiscan Spectrum using a 535 nm excitation filter (25 nm bandwidth) and 590 nm emission filter (20 nm bandwidth). Fluorescence polarization value of Calcipotriol is defined as 100%, and the relative affinity ratio of other compounds to be tested is calculated as follows: $(mP_{DMSO} - mP_{compound})/(mP_{DMSO} - mP_{Calcipotriol}) \times 100\%$.

4.3. Transcription assay

Luciferase activity assay was performed using the Dual-Luciferase Reporter Assay System (Vazyme, Nanjing, China) according to the manufacturer's instructions. HEK293 cells of 50–60% confluence were seeded in 48-well plates. Transfections were composed of 140 ng of TK-SPP × 3-Luci reporter plasmid, 20 ng of pCMX-Renilla, 30 ng of pENTER-CMV-hRXRα, and 100 ng of pCMX-VDR for each well using Lipofectamine2000 Reagent (Thermofisher, Massachusetts, USA). Six hours after transfection, test compounds were added. Luciferase activity assay was performed 48 h later using the Dual-Luciferase Assay System. Firefly luciferase activity was normalized to the corresponding Renilla luciferase activity. All the experiments were performed three times at the same condition.

4.4. CCl_4-induced mouse hepatic fibrosis model and bile duct ligation-induced cholestatic mouse liver injury model

Eight-week-old male C57BL/6 mice were purchased from the Medical School of Yangzhou University (Yangzhou, China). All animal experiments were carried out in strict accordance with the recommendations in the Guide for the Care and Use of Laboratory Animals of the National Institutes of Health and were approved by the Experimentation Ethics Review Committee of China Pharmaceutical University. All animals were housed in the specific-pathogen free animal facility with an ambient temperature of 24 ± 2 °C, air humidity of 40–70% and a 12 h dark/12 h light cycle. To set up CCl_4-induced mouse liver fibrosis model, mice received an intraperitoneal injection of a CCl_4/olive oil (1/50, v/v) mixture at a dose of 0.5 mL/kg three times weekly for 4 weeks. Control mice received vehicle (DMSO in corn oil) instead.

Bile duct ligation-induced cholestatic Mouse liver injury model was established by separating the bile duct from the portal vein and hepatic artery after the mice were anaesthetized with isoflurane, then ligated using a 6–0 suture. The sham group underwent similar laparotomy without BDL. All operations were performed under sodium pentobarbital anesthesia, and all efforts were made to minimize suffering.

4.5. Anti-fibrotic treatments

For CCl_4-induced liver fibrosis mice, treatments began after 2 weeks of CCl_4 injections, when fibrosis usually develops. DMSO, Calcipotriol (100 μg/kg body weight), compound **sw-22**, **15b**, **16i** or **28m** (500 μg/kg body weight) was administered by oral gavage five times weekly for 2 weeks. Mice were sacrificed 4 h after the final treatment to obtain serum and liver samples for blood chemistry analysis, immunofluorescence and histological staining, Western blot and qPCR assays. For BDL-induced liver fibrosis mice, treatments began after 1 weeks of laparotomy. Other treatments were similar with CCl_4-induced liver fibrosis mice but only lasted 10 days.

4.6. Ultrasound imaging

The development of liver fibrosis was monitored by high-frequency ultrasound imaging using FUJIFILM VisualSonics Vevo LAZR. Mice were anaesthetized with 2.5% isoflurane and placed on the heated Vevo mouse-handling table in a supine position. Prewarmed ultrasound transmission gel was applied to the mouse skin after removing the abdomen fur. Mice were scanned from the ventral body wall using the LZ250 real-time MicroScan transducer and the Vevo LAZR imaging system. The livers were imaged in the parasternal long axis view. The brightness of livers and kidneys was quantified by integrated density using post-processing software tool.

4.7. Blood chemistry analysis

To detect the changes of liver function of mice in each group, serum was collected by centrifugation of whole blood cell samples at 12,000 rpm at 4 °C for 10 min. Serum alanine amino transferase (ALT), aspartic transaminase (AST), and total bile acid (TBA), and calcium levels were measured using commercial kits (Rayto, Shenzhen, China).

4.8. The histological staining

For Histological Staining, liver tissues were fixed in 4% (w/v) neutral phosphatebuffered paraformaldehyde for 24 h, dehydrated, transparentized, and embedded in paraffin. Liver tissues were cut into 5 μm sections, which were stained with hematoxylin-eosin (H&E) for structured observation, or with Masson's Trichrome staining for detection of collagen deposits.

4.9. RNA extraction and quantitative real-time polymerasechain reaction (qPCR)

cDNA was generated from RNA extracts derived from cultured LX-2 cells and liver tissues using HiScript II Q RT SuperMix for Q-PCR (+ gDNA wiper Mix) (Vazyme, Nanjing, China). β-actin (human) or β-actin (mouse) was used as an internal control. Q-PCR was performed using Hieff® Q-PCR SYBR Green Master Mix (High Rox Plus) (Vazyme, Nanjing, China). Primer pairs of mRNA used are as shown in Table S2.

4.10. Western blot assay

Cell or tissue samples were lysed by a radio-immunoprecipitation assay buffer. BCA Protein Assay Kit (Beyotime, Shanghai, China) was used to determine the protein concentration in samples according to the manufacturer's protocols. The protein solution was diluted by SDS-PAGE sample loading buffer (5 ×) that contained the reducing

reagent and heated at 95 °C for 5 min. Protein was separated by 4–20% SDS-polyacrylamide gel electrophoresis (Yeasen, Shanghai, China), and then transferred to polyvinylidene fluoride (PVDF) membrane. The membranes were blocked with 5% bovine serum albumin at 37 °C for 1 h and then incubated with primary antibodies overnight at 4 °C. The membranes were washed and further incubated with a secondary antibody at room temperature for 1 h, and then detected using Tanon5200. The following primary antibodies were employed: mouse anti-α-SMA (Boster, Wuhan, China), rabbit anti-collagen I (Boster, Wuhan, China), and mouse anti-β-actin (Boster, Wuhan, China). Horseradish peroxidase-conjugated goat antirabbit/mouse IgG (Boster, Wuhan, China) was used as the secondary antibody. Image Lab 6.0.1 was used to acquire images. Cumulative densitometric analyses of the western blotting images were performed by ImageJ 1.48v.

4.11. Statistical analysis

Data were presented as means ± standard deviation (SD). Statistical significance was determined by using a two-tailed unpaired Student's *t*-test when only two value sets were compared or ANOVA for comparison between multiple groups via GraphPad Prism 7.04v. Exact *P* values are documented in the figures or figure legends. No exclusion criteria were incorporated in the design of the experiments for this study.

Declaration of competing interest

The authors declare that they have no known competing financial interests or personal relationships that could have appeared to influence the work reported in this paper.

Data availability

Data will be made available on request.

Acknowledgments

We thank the Public Platform of the State Key Laboratory of Natural Medicines for assistance with the pathological-section imaging. This work was supported by the National Natural Science Foundation of China (Nos. 82130102, 81930099, 92159304, 81773664, 81703585), the Natural Science Foundation of Jiangsu Province (No. BK20212011), the "Open Competition to Select the Best Candidates" Key Technology Program for Nucleic Acid Drugs of NCTIB (No. NCTIB2022HS01014), the "Double First-Class" University Project (No. CPU2022QZ05), the 111 Project from the Ministry of Education of China and the State Administration of Foreign Expert Affairs of China (Nos. 111-2-07 and B17047), the Fundamental Research Funds for the Central Universities of China (No. 2632022ZD11), and the Open Project of State Key Laboratory of Natural Medicines (No. SKLNMZZ202223).

Appendix A. Supplementary data

Supplementary data to this article can be found online at https://doi.org/10.1016/j.ejmech.2023.115596.

References

[1] R. Bataller, D.A. Brenner, Liver fibrosis, J. Clin. Invest. 115 (2005) 209–218.
[2] M.M. Aydın, K.C. Akçalı, Liver fibrosis, Turk. J. Gastroenterol. 29 (2018) 14–21.
[3] P. Muriel, Fighting liver fibrosis to reduce mortality associated with chronic liver diseases: the importance of new molecular targets and biomarkers, EBioMedicine 40 (2019) 35–36.
[4] D. Schuppan, M. Ashfaq-Khan, A.T. Yang, Y.O. Kim, Liver fibrosis: direct antifibrotic agents and targeted therapies, Matrix Biol. 68–69 (2018) 435–451.
[5] T. Tsuchida, S.L. Friedman, Mechanisms of hepatic stellate cell activation, Nat. Rev. Gastroenterol. Hepatol. 14 (2017) 397–411.
[6] T. Kisseleva, M. Cong, Y. Paik, D. Scholten, C. Jiang, C. Benner, K. Iwaisako, T. Moore-Morris, B. Scott, H. Tsukamoto, S.M. Evans, W. Dillmann, C.K. Glass, D. A. Brenner, Myofibroblasts revert to an inactive phenotype during regression of liver fibrosis, Proc. Natl. Acad. Sci. U. S. A. 109 (2012) 9448–9453.
[7] Y. Inagaki, I. Okazaki, Emerging insights into Transforming growth factor beta Smad signal in hepatic fibrogenesis, Gut 56 (2007) 284–292.
[8] A. Caligiuri, A. Gentilini, M. Pastore, S. Gitto, F. Marra, Cellular and molecular mechanisms underlying liver fibrosis regression, Cells (2021) 10.
[9] M. Parola, M. Pinzani, Liver fibrosis: pathophysiology, pathogenetic targets and clinical issues, Mol. Aspect. Med. 65 (2019) 37–55.
[10] D. Schuppan, Y.O. Kim, Evolving therapies for liver fibrosis, J. Clin. Invest. 123 (2013) 1887–1901.
[11] C. Leyssens, L. Verlinden, G. De Hertogh, S. Kato, C. Gysemans, C. Mathieu, G. Carmeliet, A. Verstuyf, Impact on experimental colitis of vitamin D receptor deletion in intestinal epithelial or myeloid cells, Endocrinology 158 (2017) 2354–2366.
[12] D. Bakke, J. Sun, Ancient nuclear receptor VDR with new functions: microbiome and inflammation, Inflamm. Bowel Dis. 24 (2018) 1149–1154.
[13] M. Xiong, J. Gong, Y. Liu, R. Xiang, X. Tan, Loss of vitamin D receptor in chronic kidney disease: a potential mechanism linking inflammation to epithelial-to-mesenchymal transition, Am. J. Physiol. Ren. Physiol. 303 (2012) F1107–F1115.
[14] P. Zerr, S. Vollath, K. Palumbo-Zerr, M. Tomcik, J. Huang, A. Distler, C. Beyer, C. Dees, K. Gela, O. Distler, G. Schett, J.H. Distler, Vitamin D receptor regulates TGF-β signalling in systemic sclerosis, Ann. Rheum. Dis. 74 (2015), e20.
[15] N. Ding, R.T. Yu, N. Subramaniam, M.H. Sherman, C. Wilson, R. Rao, M. Leblanc, S. Coulter, M. He, C. Scott, S.L. Lau, A.R. Atkins, G.D. Barish, J.E. Gunton, C. Liddle, M. Downes, R.M. Evans, A vitamin D receptor/SMAD genomic circuit gates hepatic fibrotic response, Cell 153 (2013) 601–613.
[16] A. Duran, E.D. Hernandez, M. Reina-Campos, E.A. Castilla, S. Subramaniam, S. Raghunandan, L.R. Roberts, T. Kisseleva, M. Karin, M.T. Diaz-Meco, J. Moscat, p62/SQSTM1 by binding to vitamin D receptor inhibits hepatic stellate cell activity, fibrosis, and liver cancer, Cancer Cell 30 (2016) 595–609.
[17] M.A. Maestro, F. Molnár, C. Carlberg, Vitamin D and its synthetic analogs, J. Med. Chem. 62 (2019) 6854–6875.
[18] M. Choi, M. Makishima, Therapeutic applications for novel non-hypercalcemic vitamin D receptor ligands, Expert Opin. Ther. Pat. 19 (2009) 593–606.
[19] L.A. Plum, H.F. DeLuca, Vitamin D, disease and therapeutic opportunities, Nat. Rev. Drug Discov. 9 (2010) 941–955.
[20] S. Fernández, M. Ferrero, Strategies for the synthesis of 19-nor-Vitamin D analogs, Pharmaceuticals (Basel) 13 (2020).
[21] G. Jones, M. Kaufmann, Update on pharmacologically-relevant vitamin D analogues, Br. J. Clin. Pharmacol. 85 (2019) 1095–1102.
[22] Y. Ma, B. Khalifa, Y.K. Yee, J. Lu, A. Memezawa, R.S. Savkur, Y. Yamamoto, S. R. Chintalacharuvu, K. Yamaoka, K.R. Stayrook, K.S. Bramlett, Q.Q. Zeng, S. Chandrasekhar, X.P. Yu, J.H. Linebarger, S.J. Iturria, T.P. Burris, S. Kato, W. W. Chin, S. Nagpal, Identification and characterization of noncalcemic, tissue-selective, nonsecosteroidal vitamin D receptor modulators, J. Clin. Invest. 116 (2006) 892–904.
[23] S. Yamada, M. Makishima, Structure-activity relationship of nonsecosteroidal vitamin D receptor modulators, Trends Pharmacol. Sci. 35 (2014) 324–337.
[24] W. Hakamata, Y. Sato, H. Okuda, S. Honzawa, N. Saito, S. Kishimoto, A. Yamashita, T. Sugiura, A. Kittaka, M. Kurihara, (2S,2'R)-analogue of LG190178 is a major active isomer, Bioorg. Med. Chem. Lett 18 (2008) 120–123.
[25] W. Shen, J. Xue, Z. Zhao, C. Zhang, Novel nonsecosteroidal VDR agonists with phenyl-pyrrolyl pentane skeleton, Eur. J. Med. Chem. 69 (2013) 768–778.
[26] M. Peräkylä, M. Malinen, K.H. Herzig, C. Carlberg, Gene regulatory potential of nonsteroidal vitamin D receptor ligands, Mol. Endocrinol. 19 (2005) 2060–2073.
[27] S. Fujii, H. Masuno, Y. Taoda, A. Kano, A. Wongmayura, M. Nakabayashi, N. Ito, M. Shimizu, E. Kawachi, T. Hirano, Y. Endo, A. Tanatani, H. Kagechika, Boron cluster-based development of potent nonsecosteroidal vitamin D receptor ligands: direct observation of hydrophobic interaction between protein surface and carborane, J. Am. Chem. Soc. 133 (2011) 20933–20941.
[28] M. Hao, S. Hou, L. Xue, H. Yuan, L. Zhu, C. Wang, B. Wang, C. Tang, C. Zhang, Further developments of the phenyl-pyrrolyl pentane series of nonsteroidal vitamin D receptor modulators as anticancer agents, J. Med. Chem. 61 (2018) 3059–3075.
[29] Z. Kang, C. Wang, Y. Tong, Y. Li, Y. Gao, S. Hou, M. Hao, X. Han, B. Wang, Q. Wang, C. Zhang, Novel nonsecosteroidal vitamin D receptor modulator combined with gemcitabine enhances pancreatic cancer therapy through remodeling of the tumor microenvironment, J. Med. Chem. 64 (2021) 629–643.
[30] C. Wang, B. Wang, L. Xue, Z. Kang, S. Hou, J. Du, C. Zhang, Design, synthesis, and antifibrosis activity in liver of nonsecosteroidal vitamin D receptor agonists with phenyl-pyrrolyl pentane skeleton, J. Med. Chem. 61 (2018) 10573–10587.
[31] C. Carlberg, F. Molnár, A. Mouriño, Vitamin D receptor ligands: the impact of crystal structures, Expert Opin. Ther. Pat. 22 (2012) 417–435.
[32] P. Gogoi, S. Seoane, R. Sigüeiro, T. Guiberteau, M.A. Maestro, R. Pérez-Fernández, N. Rochel, A. Mouriño, Aromatic-based design of highly active and noncalcemic vitamin D receptor agonists, J. Med. Chem. 61 (2018) 4928–4937.
[33] E. Thomas, J.D. Brion, J.F. Peyrat, Synthesis and preliminary biological evaluation of new antiproliferative aromatic analogues of 1α,25-dihydroxyvitamin D3, Eur. J. Med. Chem. 86 (2014) 381–393.
[34] L. Xu, A.Y. Hui, E. Albanis, M.J. Arthur, S.M. O'Byrne, W.S. Blaner, P. Mukherjee, S.L. Friedman, F.J. Eng, Human hepatic stellate cell lines, LX-1 and LX-2: new tools for analysis of hepatic fibrosis, Gut 54 (2005) 142–151.
[35] F. Saponaro, A. Saba, R. Zucchi, An update on vitamin D metabolism, Int. J. Mol. Sci. 21 (2020).
[36] Z. Kang, C. Wang, Y. Tong, Y. Li, Y. Gao, S. Hou, M. Hao, X. Han, B. Wang, Q. Wang, C. Zhang, Novel nonsecosteroidal vitamin D receptor modulator

combined with gemcitabine enhances pancreatic cancer therapy through remodeling of the tumor microenvironment, J. Med. Chem. 64 (2021) 629–643.
[37] F. Wang, Y. Yao, H.L. Zhu, Y. Zhang, Nitrogen-containing heterocycle: a privileged scaffold for marketed drugs, Curr. Top. Med. Chem. 21 (2021) 439–441.
[38] N.L. Hunter, G.R. Rao, R.E. Sherman, Flexibility in the FDA approach to orphan drug development, Nat. Rev. Drug Discov. 16 (2017) 737–738.
[39] S. Kumari, A.V. Carmona, A.K. Tiwari, P.C. Trippier, Amide bond bioisosteres: strategies, synthesis, and successes, J. Med. Chem. 63 (2020) 12290–12358.
[40] S. Nayeri, C. Carlberg, Functional conformations of the nuclear 1alpha,25-dihydroxyvitamin D3 receptor, Biochem. J. 327 (Pt 2) (1997) 561–568.
[41] C. Solomon, M. Macoritto, X.L. Gao, J.H. White, R. Kremer, The unique tryptophan residue of the vitamin D receptor is critical for ligand binding and transcriptional activation, J. Bone Miner. Res. 16 (2001) 39–45.
[42] K. Wang, S. Fang, Q. Liu, J. Gao, X. Wang, H. Zhu, Z. Zhu, F. Ji, J. Wu, Y. Ma, L. Hu, X. Shen, D. Gao, J. Zhu, P. Liu, H. Zhou, TGF-β1/p65/MAT2A pathway regulates liver fibrogenesis via intracellular SAM, EBioMedicine 42 (2019) 458–469.
[43] A. Ravichandra, R.F. Schwabe, Mouse models of liver fibrosis, Methods Mol. Biol. 2299 (2021) 339–356.
[44] N. Arroyo, L. Villamayor, I. Díaz, R. Carmona, M. Ramos-Rodríguez, R. Muñoz-Chápuli, L. Pasquali, M.G. Toscano, F. Martín, D.A. Cano, A. Rojas, GATA4 induces liver fibrosis regression by deactivating hepatic stellate cells, JCI Insight (2021) 6.
[45] Y. Lurie, M. Webb, R. Cytter-Kuint, S. Shteingart, G.Z. Lederkremer, Non-invasive diagnosis of liver fibrosis and cirrhosis, World J. Gastroenterol. 21 (2015) 11567–11583.
[46] M.T. Heller, M.E. Tublin, The role of ultrasonography in the evaluation of diffuse liver disease, Radiol. Clin. 52 (2014) 1163–1175.
[47] X. Yang, L. Ma, R. Wei, T. Ye, J. Zhou, M. Wen, R. Men, R.I. Aqeilan, Y. Peng, L. Yang, Twist1-induced miR-199a-3p promotes liver fibrosis by suppressing caveolin-2 and activating TGF-β pathway, Signal Transduct. Targeted Ther. 5 (2020) 75.
[48] N. Coppola, A. Perna, A. Lucariello, S. Martini, M. Macera, M.A. Carleo, G. Guerra, V. Esposito, A. De Luca, Effects of treatment with Maraviroc a CCR5 inhibitor on a human hepatic stellate cell line, J. Cell. Physiol. 233 (2018) 6224–6231.
[49] B.M. Wu, J.D. Liu, Y.H. Li, J. Li, Margatoxin mitigates CCl4-induced hepatic fibrosis in mice via macrophage polarization, cytokine secretion and STAT signaling, Int. J. Mol. Med. 45 (2020) 103–114.
[50] N.A. Salem, A. Hamza, H. Alnahdi, N. Ayaz, Biochemical and molecular mechanisms of platelet-rich plasma in ameliorating liver fibrosis induced by dimethylnitrosurea, Cell. Physiol. Biochem. 47 (2018) 2331–2339.